2. EXPLANATORY NOTES[1]

Shipboard Scientific Party[2]

INTRODUCTION

This chapter presents the shipboard methods used to obtain the results presented in the site chapters in this volume. The separate sections of the site chapters were written by the shipboard scientific specialists for each scientific discipline (see list of participants at the front of this volume).

Coring techniques and core handling, including the numbering of sites, holes, cores, sections, and samples, were the same as those described in previous *Initial Reports* volumes of the *Proceedings of the Ocean Drilling Program.* Following Leg 171B, the cores were transferred in refrigerated containers from the ship to cold storage at the Bremen Core Repository of the Ocean Drilling Program (ODP), in Bremen, Germany.

LITHOSTRATIGRAPHY

The description of sedimentary units recovered during Leg 171B includes estimates of sediment composition, sedimentary structures, deformational structures, drilling disturbance, presence and type of body and trace fossils, bioturbation, consolidation/lithification, and diagenetic alteration. Depending on the scale of lithologic variability and because of the large amount of core recovered, observations of the shipboard sedimentologists and the stratigraphic positions of routine samples were recorded either for an entire core on a barrel sheet, or for each section on standard ODP Visual Core Description (VCD) forms. Copies of the VCD forms and handwritten barrel sheets are available upon request from ODP. The sedimentologic data for each core were summarized on core-description forms (Fig. 1), or "barrel sheets," that are presented with the core photographs in Section 4 (this volume). The forms were generated using AppleCORE software (Mike Ranger, v. 7.5, 1989–1996).

Lithology

The composition of sediment recovered is depicted in the "Lithology" column of the barrel sheets, using the symbols shown in Figure 2. Individual beds ≤10 cm thick are not plotted unless they represent exceptional lithologies or are otherwise considered important, but they are noted in the "Lithologic Description" section (this chapter). When an interval contains sediment that is best described as a mixture of two or more of the lithologies shown in Figure 2 (e.g., a nannofossil-rich ooze containing common foraminifers and radiolarians), the lithologic symbols of the end-members are plotted side by side. The width occupied by each symbol represents the relative abundance of the three most common constituents, provided they each constitute >10% of the mixture. Constituents representing ≤10% (or potentially >10% if more than three constituents are mixed) are not depicted graphically but are listed in the lithologic description.

Sedimentary and Biogenic Structures

Physical and biological structures are depicted in the "Physical Structures," "Ichnofossils," and "Fossils" columns, using the symbols shown in Figure 2. Discrete sedimentologic features, including primary depositional structures such as ripples and graded beds, and syn- and postdepositional deformation, are indicated in the "Physical Structures" column of the barrel sheets. Other primary sedimentologic and diagenetic features, such as distinct laminae, ash layers, chert, and glauconite, are depicted in the "Lithologic Accessories" column. Discrete ichnofossils and overall bioturbation are plotted in the "Ichnofossils" column. The intensity of bioturbation, plotted in the "Ichnofossils" column of the barrel sheets, uses conventional categories (slight, moderate, and heavy) that we recognized based on the following criteria:

Slight = primary depositional contacts that are largely preserved but are cut by discrete burrows;
Moderate = fabric that is dominated by biogenic structures, but primary depositional contacts are partially preserved; and
Heavy = biogenic fabric that has no primary depositional contacts preserved.

Natural structures (physical and biological) and disturbance created by the coring process can be difficult to distinguish unambiguously. We attempt to convey the maximum amount of information without confusing interpretation with observation. Where bioturbation is inferred (e.g., in some homogeneous intervals), we used dashed lines to show that the sedimentary fabric is being interpreted, whereas solid lines are used to show intervals in which burrows can be observed. Recognizable body fossils are depicted in the "Fossils" column.

Sediment Disturbance

Sediment disturbance resulting from the coring process is illustrated in the "Core Disturbance" column on the core-description forms (using symbols shown in Fig. 2). The degree of drilling disturbance for soft sediments is described using the following categories:

Slightly disturbed = bedding contacts are slightly bent;
Moderately disturbed = bedding contacts are extremely bowed;
Highly disturbed = bedding is completely disturbed and, in some cases, shows symmetrical diapir-like or flow structures; and
Soupy = intervals are water-saturated and have lost all original structure.

Fragmentation caused by the drilling process in indurated sediments and rock is described using the following categories:

Slightly fragmented = core pieces are in place with little drilling slurry or breccia;

[1]Norris, R.D., Kroon, D., Klaus, A., et al., 1998. *Proc. ODP, Init. Repts.,* 171B: College Station, TX (Ocean Drilling Program).
[2]Shipboard Scientific Party is given in the list preceding the Table of Contents.

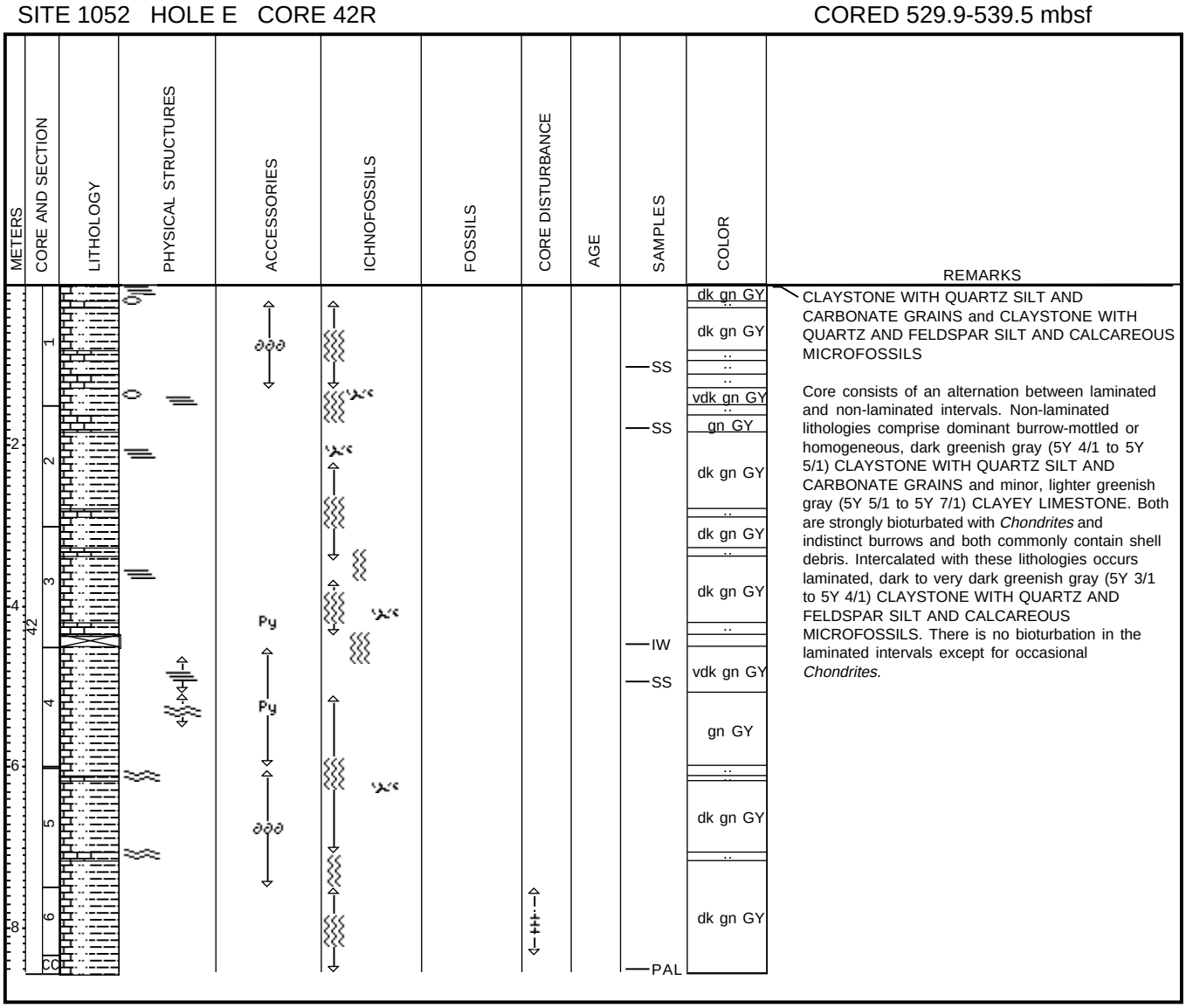

Figure 1. Core-description form (barrel sheet) used for sediments and sedimentary rocks. The 171B barrel sheets are included in Section 4 (this volume).

Moderately fragmented = core pieces are in place or partly displaced, but the original orientation is preserved or recognizable (drilling slurry may surround fragments);
Highly fragmented = core pieces are from the interval cored and are probably in correct stratigraphic sequence (although they may not represent the entire section), but the original orientation is completely lost; and
Drilling breccia = core pieces have lost their original orientation and stratigraphic position and may be mixed with drilling slurry.

As for bioturbation, solid lines in the column indicate intervals where features diagnostic of drilling disturbance are observed; dashed lines denote intervals where disturbance is inferred.

Samples and Close-Up Photographs

The stratigraphic position of various samples taken for shipboard analysis and the location of close-up photographs are indicated in the "Samples" column of the barrel sheets, according to the following codes:

SS = smear-slide sample;
CAR = carbonate sample;
XRD = X-ray-diffraction sample;
XRF = X-ray-fluorescence sample;
TS = thin-section sample;
PAL = biostratigraphy (paleontology) sample;
PHO = close-up photograph;
IW = interstitial-water whole-round sample;
WR = other whole-round sample; and
SAM = other sample.

In the "Remarks" column, selected smear slides taken from a dominant lithology are designated as "SD"; those taken from a minor lithology are designated as "SM."

Color

Visual estimates of the color (hue, chroma, and value) were made using Munsell Soil Color Charts (1975) or Rock Color Charts (1991) and are reported as standard Munsell colors in the "Color" column of

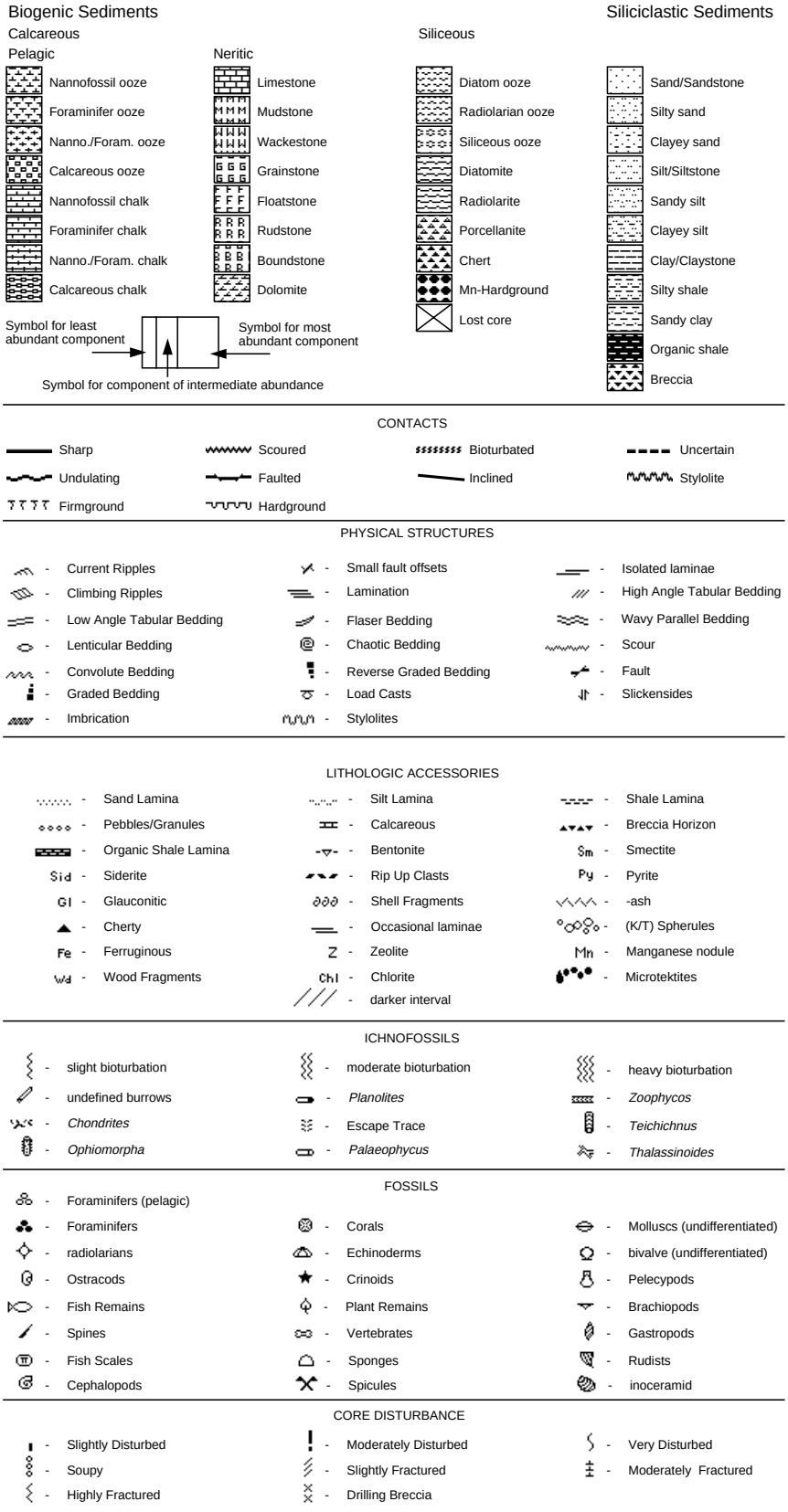

Figure 2. Key to patterns used in the “Lithology” column and symbols used in the “Physical Structures,” “Accessories,” “Ichnofossils,” “Fossils,” and “Core Disturbance” columns on the core-description form, shown in Figure 1.

the barrel sheets. Because redox reactions can lead to rapid color changes in deep-sea sediments exposed to the atmosphere, color was estimated as soon as possible, and cores were covered with clear plastic from the time they were split until after all color measurements were completed. In addition, where core disturbance allowed, all cores were scanned at 5-cm intervals using a Minolta CM-2002 spectrophotometer, which returned Munsell color codes and reflectance in thirty-one 10-nm-wide bands of the visible spectrum (400–700 nm). These data are included in Section 4 (this volume).

Smear Slides

A table summarizing data from smear-slide analyses is included after the barrel sheets and core photographs from each site in Section 5 (on CD-ROM, back pocket, this volume). Routine observations that were made include sample location, whether the lithology sampled was dominant or minor, an estimate of grain-size distribution, and estimates of the relative abundance of various components. To characterize the relative abundance of different grain types, we de-emphasized percentage estimates (Rothwell, 1989) but maintained semiquantitative categories to facilitate the interpretation of plots of stratigraphic trends in sediment composition as follows:

0 = none (not present);
1 = trace (0%–2%);
2 = rare (2%–10%);
3 = common (10%–25%);
4 = abundant (25%–50%); and
5 = dominant (>50%).

We feel that these categories reflect our precision. However, the subjective nature of the observations should be kept in mind, especially as the tables are a compilation of the observations of many workers. Smear slides and smear-slide tables were reviewed for internal consistency and for correct sedimentologic nomenclature, where time permitted.

Lithologic Description—Text

The lithologic description that appears in the "Remarks" column of the barrel sheet is based on the results of visual core description and smear-slide analysis. It consists of three parts: (1) a heading that lists all the major sediment lithologies observed in the core; (2) a general description of these sediments including colors and any other significant features in the core; and (3) descriptions and locations of thin, interbedded, or minor lithologies, as well as any clarifying information regarding sediment disturbance produced by natural processes or the drilling/coring process.

Classification of Sediments and Sedimentary Rocks

Leg 171B used a slightly modified version of the ODP sediment classification scheme (Mazzullo et al., 1988) for sediments. By this scheme (Fig. 3), the lithologies recovered during Leg 171B are classified either as granular or chemical. Granular sediment contains any of four types of grains: pelagic, neritic, volcaniclastic, or siliciclastic. The pelagic grains most commonly observed are open-marine calcareous and, to a lesser extent, siliceous microfossils (foraminifers, radiolarians, calcareous nannofossils, diatoms, siliceous sponge spicules, and others). It also includes carbonate and opal grains derived from these fossils by diagenesis. Any silt- or clay-sized calcareous grains are referred to in this volume as "carbonate."

Neritic grains comprise shallow-water carbonate debris including carbonate rock fragments and shallow-water carbonate fossils. Siliciclastic grains comprise mineral and rock fragments and include clay minerals. Volcaniclastic grains recovered during this leg are volcanic ash grains. The relative proportions of the four components are used to define the major classes of granular sediments in the cores. Sediment that contains >50% biogenic grains is classified as neritic or pelagic, depending on which type of biogenic component dominates (Fig. 3). Sediment that contains <50% biogenic grains is classified as siliciclastic or volcaniclastic, depending on whether volcanic or siliciclastic grains dominate (Fig. 3). We have omitted the term "mixed sediment," used by Mazzullo et al. (1988), and use only the four classes, pelagic, neritic, volcaniclastic, and siliciclastic.

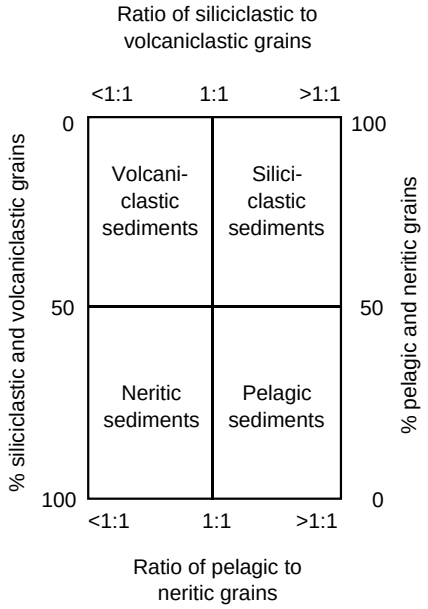

Figure 3. Classes of granular sediment (modified from Mazzullo et al., 1988).

Chemical sediment is composed of minerals that formed by inorganic processes and, for Leg 171B sediment, includes principally manganese/phosphate nodules and coatings, pyrite, and glauconite. Sediments are named according to their mineral composition.

Principal Names of Granular Sediment

Each granular sediment class has a unique set of principal names, outlined in Table 1. For pelagic sediment, the principal name describes the composition and degree of consolidation using the following terms:

Ooze = unconsolidated calcareous and/or siliceous biogenic sediments;
Chalk = firm biogenic sediment composed predominantly of calcareous biogenic grains;
Limestone = hard pelagic sediment composed predominantly of calcareous pelagic grains;
Diatomite = firm pelagic sediment composed predominately of siliceous diatoms;
Chert = vitreous or lustrous, conchoidally fractured, highly indurated rock composed predominately of diagenetic silica (either opal-CT or quartz); and
Porcellanite = well-undurated rock with abundant diagenetic silica (either opal-CT or quartz) that is less hard, lustrous, or brittle than chert (in part, such rocks may represent mixed sedimentary rock).

For neritic sediment recovered during Leg 171B, the principal name describes the texture and fabric using the terminology of Dunham (1962) as follows:

Table 1. Outline of granular-sediment classification scheme.

Sediment class	Major modifiers	Principal names	Minor modifiers
Pelagic sediment	1. Composition of pelagic and neritic grains present in major amounts. 2. Texture of clastic grains present in major amounts.	1. Ooze 2. Chalk 3. Limestone 4. Radiolarite 5. Diatomite 6. Spiculite 7. Porcellanite 8. Chert	1. Composition of pelagic and neritic grains present in minor amounts. 2. Texture of clastic grains present in minor amounts.
Neritic sediment	1. Composition of neritic and pelagic grains present in major amounts. 2. Texture of clastic grains present in major amounts.	1. Grainstone 2. Packstone	1. Composition of neritic and pelagic grains present in minor amounts. 2. Texture of clastic grains present in minor amounts.
Siliciclastic sediment	1. Composition of all grains present in major amounts. 2. Grain fabric (gravels only) 3. Grain shape (optional). 4. Sediment color (etc.).	1. Sand 2. Silt 3. Clay	1. Composition of all grains present in minor amounts. 2. Texture and composition of siliciclastic grains present as matrix (for coarse-grained clastic sediments).
Volcaniclastic sediment	1. Composition of all volcaniclasts present in major amounts. 2. Composition of all pelagic and neritic grains present in major amounts. 3. Texture of siliciclastic grains present in major amounts.	1. Ash/tuff	1. Composition of all volcaniclasts present in minor amounts. 2. Composition of all neritic and pelagic grains present in minor amounts. 3. Texture of siliciclastic grains present in minor amounts.

Note: Classification scheme is from Mazzullo et al. (1988).

Grainstone = grain-supported fabric, no mud, grains <2 mm in size; and
Packstone = grain-supported fabric with intergranular mud grains <2 mm in size.

The composition of neritic grains includes the following:

Ooids = spherical or elliptical, non-skeletal particles, <2 mm in diameter, having a central nucleus surrounded by a rim with concentric or radial fabric;
Bioclasts = fragment of skeletal remains; and
Peloids = micritized carbonate particles of unknown origin.

For siliciclastic sediment, the principal name describes the texture and is assigned according to the following guidelines:

1. Textural groups (gravel, sand, silt, and clay) and subgroups (fine sand, coarse silt, etc.) from the Udden-Wentworth grain-size scale (Wentworth, 1922) are used as the principal names of siliciclastic sediment. The boundary between silt and clay was placed at 2 µm, as suggested by Doeglas (1968; Fig. 4).
2. When two or more textural groups or subgroups are present in a siliciclastic sediment, they are listed as principal names in order of increasing abundance.
3. The suffix "-stone" is affixed to the principal names sand, silt, and clay if the sediment is lithified.

For volcaniclastic sediment, we use the term "ash" to describe sediment that contains >50% sand and finer grained volcanic grains. The composition is either "vitric" (isotropic grains) or "altered" (weakly birefringent grains).

Major and Minor Modifiers for Granular Sediment

The principal name of a sediment class is preceded by major modifiers and is followed by minor modifiers (preceded by the term "with") that describe the lithology of the granular sediment in greater detail (Table 1). The most common use of major and minor modifiers is to describe the composition and texture of grain types that are present in major (>25%) and minor (10%–25%) proportions. Note that modifiers are always listed in order of increasing abundance. For example, an unconsolidated pelagic sediment containing 30% clay, 15% foraminifers, and 55% nannofossils would be called a clayey nannofossil ooze with foraminifers (Mazzullo et al., 1988).

X-ray Diffraction Analysis

Selected samples were taken for qualitative mineral analysis by XRD using a Philips diffractometer with CuKα radiation at 40 kV and 35 mA, with a focusing graphite monochromator and the following slit settings:

focus = fine;
irradiated length = 12 mm;
divergence slit = automatic;
receiving slit = 0.2 mm;
step size = 0.02°2θ;
count time per step = 1 s;
scanning rate = 2°2θ/min;
rate meter time constant = 0.2 s;
spinner = off;
monochromator = on; and
scan = continuous.

Bulk samples were freeze-dried, ground with an agate mortar and pestle, and packed in sample holders, which, together with the ship's movement, probably imparted some orientation to the mineral powder. These samples were scanned from 2° to 70°2θ.

Samples analyzed for clay mineral determination were neither freeze-dried nor ground; they were soaked with demineralized water. The suspension was decarbonated with dilute hydrochloric acid (HCl) on a magnetic stirrer until a slightly acidic pH was reached. The sample was then washed with demineralized water to remove acid and salt until the suspension ceased to flocculate. If repeated washing did not affect deflocculation, Calgon was added to the suspension. Before clay separation by settling, all suspensions were treated ultrasonically for 10 min. After 1 hr of settling, an aliquot of the suspension was pipetted off from a 1-cm water depth and put into

Millimeters (mm)	Micrometers (μm)	Phi (ϕ)	Size class	
256		-8.0	Cobble	Gravel
84		-6.0	Pebble	
4		-2.0	Granule	
2.00		-1.0	very coarse Sand	
1.00		0.0	coarse Sand	
0.50	500	1.0	medium Sand	Sand
0.25	250	2.0	fine Sand	
0.125	125	3.0	very fine Sand	
0.0625	63	4.0	very coarse Silt	
0.031	31	5.0	coarse Silt	
0.0156	15.6	6.0	medium Silt	Silt
0.0078	7.8	7.0	fine silt	
0.0039	3.9	8.0	very fine silt	
0.0002	2.0	9.0	Clay	

Figure 4. Grain-size scale used for siliciclastic sediments (modified from Wentworth, 1922). Silt/clay boundary is according to Doeglas (1968).

a Milipore filtration apparatus with a 0.45-μm membrane filter. The clay cake was transferred from the membrane filter to a glass slide by placing the filter on the slide and rolling the paper with a small glass beaker. Once air-dried, clay samples were scanned from 2° to 35°2θ and then placed over ethylene glycol in a desiccator at room temperature for 24 hr before being scanned again. The raw data files of all diffractometer runs are on CD-ROM (back pocket, this volume). Clay mineral identification broadly followed the procedures of Moore and Reynolds (1989). Selected diffractograms illustrating which peaks we associated with various minerals are shown in the site chapters.

X-ray Fluorescence Analysis

Selected sediments were analyzed for major elements during Leg 171B. Before analysis, samples were crushed in the shipboard Spex 8510 Shatterbox using a tungsten carbide barrel. This process produces some tantalum and massive tungsten contamination of the sample.

A fully automated ARL 8420 wavelength-dispersive XRF system was used to determine the abundances of major oxides in whole-rock samples. Analyses of these major oxides were performed on lithium borate glass disks doped with lanthanum as a "heavy adsorber" (Norrish and Hutton, 1969). The disks were prepared from 500 mg of rock powder, ignited for 2 hr at about 1030°C, and mixed with 6.000 g of dry flux consisting of 80% lithium tetraborate and 20% La_2O_3. This mixture was then melted at 1150°C in a platinum-gold crucible for about 10 min and, using a Claisse Fluxer, was poured into a platinum-gold mold. This XRF was calibrated using between 7 and 10 standards for each element. Results have been reported as the weight percentage of SiO_2, TiO_2, Al_2O_3, Fe_2O_3, MnO, MgO, CaO, Na_2O, K_2O, P_2O_5, and the sum of these oxide concentrations.

Systematic errors from short- or long-term fluctuations in X-ray tube intensity were corrected by normalizing the measured intensities of the samples to that of a drift standard that is always run together with a set of six samples. To reduce weighing errors, two glass disks may have been prepared for each sample. Because it can be a major source of error, the weighing process was performed with particular care.

BIOSTRATIGRAPHY

Preliminary age assignments were based on biostratigraphic analyses of calcareous nannofossils, planktonic foraminifers, and radiolarians. Paleodepth interpretations were based on benthic foraminifers. Age constraints for calcareous nannofossil and planktonic foraminifer datums were achieved by examining one sample per section of core (a sample spacing of ~1.5 m) in the A Hole. In addition, examination of the core-catcher material in every hole for calcareous nannofossil content allowed for a quick initial age estimate to be made. Core-catcher material also was selectively examined for planktonic foraminifer and radiolarian content. Because of the time-consuming nature of processing material for radiolarians, fewer samples were taken per core than for other microfossil groups (one sample per 9.5 m of core). The preservation, abundance, and zonal assignment for each sample and for each microfossil group are recorded in the stratigraphic site summary sheets.

In previous shipboard studies, materials examined for planktonic foraminifers and radiolarians have been limited to core-catcher material because of time constraints. We have adopted the strategy used previously by Mayer, Pisias, Janecek, et al. (1992) for Leg 138 and Curry, Shackleton, Richter, et al. (1995) for Leg 154 in concentrating efforts on one of the three holes cored at each site instead of all three. Hole-to-hole correlations were achieved using calcareous nannofossil datums obtained from core-catcher analysis and through data obtained using multisensor track analysis.

Age estimates of biostratigraphic data were calibrated to the magnetic polarity time scale of Cande and Kent (1995; Tables 2–4). The time scale of Berggren et al. (1995) was applied to the Cenozoic datums. Age estimates for this time interval for both calcareous nannofossil and planktonic foraminifer datums were obtained primarily from Berggren et al. (1995; Fig. 5). Correlation of Cenozoic calcareous nannofossil and planktonic foraminifer datums with radiolarian datums was estimated using the time scale of Berggren et al. (1995) either through interpolation from the nearest geomagnetic reversal boundary or through interpolation using other biostratigraphic datums.

The time scale of Gradstein et al. (1995) was used for the Cretaceous. Age estimates for the majority of Late Cretaceous calcareous nannofossil and planktonic foraminifer datums were taken from Erba et al. (1995; Fig. 5; Table 3). The first occurrences of *Abathomphalus mayaroensis, Micula prinsii, M. murus, and Nephrolithus frequens* were diachronous in nature. Therefore, some error could occur when using these datums for sedimentation rate estimates and chronostratigraphy.

Confusion exists in the definition of the Paleocene/Eocene boundary. Traditionally, the Paleocene/Eocene boundary has been placed at the calcareous nannofossil Zone NP9/NP10 (CP8b/CP9a) boundary, based on the first appearance of *Tribrachiatus bramlettei.* However, a recent paper by Bybell and Self-Trail (1995) resulted in the placement of *T. bramlettei* in synonymy with *Rhomboaster cuspis*, which, in turn, required a change in the placement of the Paleocene/Eocene boundary. This confusion among nannofossil workers about what actually defines the Paleocene/Eocene boundary marker species is reflected in Berggren et al. (1995; Fig. 5), where the Paleocene/Eocene boundary is represented by a broad gray band from 54.6 to 55.5 Ma. Because of this uncertainty, for Leg 171B, the last appearance of *Fasciculithus* spp., a genus thought to disappear approximately around the Paleocene/Eocene boundary, was used as a proxy for the Paleocene/Eocene boundary. Additionally, the last appearance of *Morozovella velascoensis* and a worldwide recognizable benthic foraminifer extinction event were used to help corroborate the placement of the Paleocene/Eocene boundary.

Table 2. Cenozoic and Mesozoic calcareous nannofossil datums.

Event	Zone (base)	Age (Ma)	Reference
B Acme *Emiliania huxleyi*		0.085	2
B *Emiliania huxleyi*	CN15	0.248	2
T *Pseudoemiliania lacunosa*	CN14b	0.408	2
B *Gephyrocapsa parallela*		0.94	2
Reentrance medium *Gephyrocapsa* spp.	CN14a?	0.97	2
T Large *Gephyrocapsa* spp.		1.18	2
B Large *Gephyrocapsa* spp.		1.40	2
T *Helicosphaera sellii*		1.41	2
T *Calcidiscus macintyrei*		1.65	2
B *Gephyrocapsa caribbeanica*	CN13b?	1.71	2
Pleistocene/Pliocene boundary		1.71	
T *Discoaster brouweri*	CN13a	1.95	2
B Acme *Discoaster triradiatus*		2.00	2
T *Discoaster pentaradiatus*	CN12d	2.36	2
T *Discoaster surculus*	CN12c	2.51	2
T *Discoaster tamalis*	CN12b	2.82	2
T *Sphenolithus* spp.	CN12a	3.62	2
T *Reticulofenestra pseudoumbilicus*	CN12a	3.83	2
T *Amaurolithus* spp.	CN11	4.50	2
T *Ceratolithus acutus*		5.04	3
B *Ceratolithus rugosus*	CN10c	5.05	2
B *Ceratolithus acutus*	CN10b	5.09	2
T *Triquetrorhabdulus rugosus*		5.23	2
Pliocene/Miocene boundary		5.30	
T *Discoaster quinqueramus*	CN10a	5.6	1
T *Amaurolithus amplificus*		5.9	1
B *Amaurolithus amplificus*		6.6	1
T Paracme *R. pseudoumbilicus*		6.8	4
B *Amaurolithus primus*	CN9b	7.2	1
T *Discoaster loeblichii*		7.4	1
T *Minylitha convalis*		7.8	1
B *Discoaster berggrenii*	CN9a	8.6	1
B *Discoaster loeblichii*		8.7	1
B Paracme *R. pseudoumbilicus*		8.8	4
T *Discoaster bollii*		9.1	1
T *Catinaster calyculus*		9.36	3
T *Discoaster hamatus*	CN8a	9.4	1
B *Minylitha convallis*		9.5	1
B *Discoaster neohamatus*		9.6	4
B *Discoaster hamatus*	CN7	10.7	1
T *Coccolithus miopelagicus*		11.0	3
B *Catinaster coalitus*	CN6	11.3	1
T *Discoaster kugleri*		11.5	1
B *Discoaster kugleri*		11.8	1
T *Coronocyclus nitescens*		12.1	4
B *Calcidiscus macintyrei* >11 µm		12.3	4
B *Triquetrorhabdulus rugosus*		13.2	1
T *Calcidiscus premacintyrei*		12.7	4
T *Discoaster signus*		12.7	4
T *Sphenolithus heteromorphus*	CN5a	13.6	1
T *Helicosphaera ampliaperta*	CN4	15.6	1
B *Discoaster signus*		16.2	4
T Abundant *Discoaster deflandrei*		16.2	4
B *Calcidiscus premacintyrei*		17.4	5
B *Sphenolithus heteromorphus*	CN3	18.2	1
T *Sphenolithus belemnos*		18.3	1
B *Sphenolithus belemnos*	CN2	19.2	1
T *Triquetrorhabdulus carinatus*		23.1	1
T *Triquetrorhabdulus serratus*		23.2	1
T *Sphenolithus umbrellus*		23.6	1
T *Sphenolithus capricornutus*		23.7	1
B *Discoaster druggi*	CN1c	23.3	6
T *Sphenolithus delphix*		23.8	1
Miocene/Oligocene boundary		23.8	
T *Dictyococcites bisectus*	CN1c	23.9	1
B *Sphenolithus delphix*		24.3	1
T *Zygrhablithus bijugatus*		24.5	1
T *Sphenolithus ciperoenis*	CN1a	24.75	1
T *Sphenolithus distentus*	CP19b	27.5	1
T *Sphenolithus predistentus*		27.5	1
T *Sphenolithus pseudoradians*		29.1	1
B *Sphenolithus ciperoensis*	CP19a	29.9	1
B *Sphenolithus distentus*	CP18	31.5-33.1	1
T *Reticulofenestra umbilicus*	CP17	32.3	1
T *Coccolithus formosus*	CP16c	32.8	1
T *Chiasmolithus oamaruensis*		33.7	1
Oligocene/Eocene boundary		33.7	
T *Discoaster saipanensis*	CP16a	34.2	1
T *Discoaster barbadiensis*	CP16a	34.3	1
T *Cribrocentrum reticulatum*		35.0	1
B *Isthmolithus recurvus*		36.0	1
T *Calcidiscus protoannulus*		36.8	7
B *Chiasmolithus oamaruensis*	CP15	37.0	1
T *Chiasmolithus grandis*	CP15	37.1	1

Event	Zone (base)	Age (Ma)	Reference
B *Dictyococcites bisecta*		38.0	1
T *Chiasmolithus solitus*	CP14b	40.4	1
B *Dictyococcites hesslandii*		41.8	7
T *Nannotetrina fulgens*		43.1	1
T *Blackites gladius*		43.4	1
B *Reticulofenestra umbilicus*	CP14a	43.7	1
T *Chiasmolithus gigas*	CP13c	44.5	1
B *Chiasmolithus gigas*	CP13b	46.1	1
B *Nannotetrina fulgens*	CP13a	47.3	1
T *Discoaster lodoensis*		47.9	1
B *Rhabdosphaera inflata*		48.5	1
B *Nannotetrina* spp.		49.2	8
B *Discoaster sublodoensis*	CP12	49.7	1
T *Tribrachiatus orthostylus*		50.6	1
B *Discoaster lodoensis*	CP10	52.85	1
T *Sphenolithus radians*		53.1	1
T *Tribrachiatus contortus*		53.6	1
B *Tribrachiatus orthostylus*		53.6	1
B *Discoaster diastypus*	CP9a	53.9	8
T *Ericsonia robusta*		54.0	8
B *Tribrachiatus contortus*	CP9a	54.3	1
Eocene/Paleocene boundary		54.5	
B *Tribrachiatus (Rhomboaster) bramlettei*		55.0	8
B *Rhomboaster* spp.		55.1	8
T *Fasciculithus tympaniformis*		55.33	1
B *Camplyosphaera eodela*	CP8b	55.5	1
B *Discoaster multiradiatus*	CP8a	56.2	1
B *Discoaster okadai*		56.8	1
B *Discoaster nobilis*	CP7	56.9	1
B *Heliolithus riedelii*		57.3	1
T *Heliolithus kleinpellii*		56.6	8
B *Discoaster mohlerii*	CP6	57.5	1
B *Sphenolithus anarrhopus*		58.4	1
T *Chiasmolithus danicus*		57.5	9
B *Heliolithus kleinpellii*	CP5	58.4	1
B *Heliolithus cantabriae*		58.2	8
T *Fasciculithus pileatus*		58.6	8
T *Cruciplacolithus tenuis*		58.6	9
B *Fasciculithus* spp.		59.2	8
B *Sphenolithus primus*		60.6	1
B *Chiasmolithus bidens*		60.7	1
B *Ellipsolithus macellus*	CP3	62.2	1
B *Chiasmolithus danicus*	CP2	63.8	1
B *Cruciplacolithus tenuis*	CP1b	64.5	1
B *Cruciplacolithus primus*		64.8	1
B *Biantholithus sparsus*		65.0	1
T Cretaceous taxa	CP1a	65.0	1
Tertiary/Cretaceous boundary		65.0	
B *Micula prinsii*		66.0	10
B *Nephrolithus frequens* (low latitude)		67.2	10
B *Micula murus*		68.5	10
T *Reinhardtites levis*		69.4	10
T *Quadrum trifidum*		71.3	10
Maastrichtian/Campanian boundary		71.3	
T *Tranolithus phacelosus*		71.6	10
T *Aspidolithus parcus*		74.6	10
T *Eiffellithus eximius*		75.3	10
T *Lithastrinus grillii*		75.1	10
B *Quadrum trifidum*		76.1	10
B *Quadrum sissinghii*		77.1	10
B *Ceratolithoides aculeus*		78.5	10
T *Bukryaster hayii*		79.8	10
T *Marthasterites furcatus*		80.6	10
B *Ceratolithoides verbeekii*		82.0	10
B *Aspidolithus parcus constrictus*		83.5	10
Campanian/Santonian boundary		83.5	
B *Calculites obscurus*		83.8	10
B *Lucianorhabdus cayeuxii*		84.8	10
T *Lithastrinus septenarius*		84.9	10
B *Lithastrinus grillii*		85.8	10
Santonian/Coniacian boundary		85.8	
B *Reinhardtites anthophorus*		85.8	10
B *Micula decussata*		87.2	10
Coniacian/Turonian boundary		89.0	
B *Marthasterites furcatus*		89.3	10
B *Lucianorhabdus maleformis*		91.0	10
B *Eiffellithus eximius*		91.0	10
B *Quadrum gartnerii*		93.5	10
Cenomanian/Turonian boundary		93.5	
T *Corollithion kennedyi*		93.9	10

Table 2 (continued).

Event	Zone (base)	Age (Ma)	Reference
T *Rhagodiscus asper*		93.9	10
T *Axopodorhabdus albianus*		93.9	10
T *Microstaurus chiastius*		94.4	10
B *Microrhabdulus decoratus*		95.2	10
B *Lithraphidites acutus*		95.2	10
B *Corollithion kennedyi*		97.4	10
Albian/Cenomanian boundary		98.9	
T *Hayesites albiensis*		99.0	10
T *Rucinolithus irregularis*		99.0	10
B *Eiffellithus turriseiffelii*		101.7	10
B *Eiffelithus* spp. (small)		103.8	10
B *Axopodorhabdus albianus*		106.5	10
B *Tranolithus phacelosus*		106.5	10
B *Cribrosphaerella ehrenbergii* (sensu Erba)		110.3	10
Aptian/Albian boundary		112.2	
B *Prediscosphaera columnata* (<5 µm)		112.5	10
T *Assipetra intracretacea*		113.0	10
B *Hayesites albiensis*		114.0	10
T *Micrantholithus hoschulzii*		114.2	10
T *Nannoconus st. steinmanii*		114.2	10
B *Braarudosphaera africana*		118.2	10
B *Stoverius achylosum*		118.2	10
B *Eprolithus floralis*		119.0	10
B *Rhagodiscus angustus*		119.9	10
T *Nannoconid paracme*		120.5	10
Barremian/Aptian boundary		121.0	
B *Rucinolithus irregularis*		121.1	10
B *Flabellites oblongus*		121.1	10

Notes: B = base; T = top. References 3 through 9 have been calibrated to the time scale of Berggren et al. (1995). References are as follows: 1 = Berggren et al. (1995); 2 = Sigurdsson, Leckie, Acton, et al. (1997); 3 = Curry, Shackleton, Richter, et al. (1995); 4 = Raffi and Flores (1995); 5 = Gartner (1992); 6 = Berggren et al. (1985b); 7 = Backman (1987); 8 = Backman (1986); 9 = Berggren et al. (1985a); 10 = Erba et al. (1995).

Calcareous Nannofossils

The zonal scheme of Bukry (1973, 1975; zonal code numbers added and modified by Okada and Bukry, 1980) was used for Cenozoic calcareous nannofossils, and the zonal scheme of Sissingh (1977), modified by Perch-Nielsen (1985), was used for Cretaceous calcareous nannofossils. Both of these zonations represent a general framework for the biostratigraphic classification of mid- to low-latitude assemblages. Okada and Bukry's (1980) Cenozoic and Sissingh's (1977) Cretaceous zonal schemes, together with the geomagnetic polarity time scale, are presented in Figure 5.

Cenozoic biostratigraphic events, which include but are not limited to the zonal indicators of Okada and Bukry (1980), are listed in Table 2. Note that in some cases, more than one biostratigraphic event was used to delineate a zonal or subzonal boundary (e.g., CP9a/CP9b). In such cases, those zonal markers indicative of low- to mid-latitude regimes were considered to be the most reliable as marker species. Special attention should be given to the Paleocene/Eocene boundary of Berggren et al. (1995; Fig. 5). Questionable placement of the boundary arises from taxonomic ambiguities in both the calcareous nannofossil zonation and the planktonic foraminifer zonal scheme. Because of these ambiguities, for Leg 171B, it was decided that the last appearance of calcareous nannofossil species belonging to the genus *Fasciculithus*, rather than the first appearance of *Rhomboaster* spp., would be used as a proxy for the Paleocene/Eocene boundary.

Mesozoic biostratigraphic events, based primarily on the zonation of Perch-Nielsen (1985) and modified by Erba et al. (1995), along with the stage boundary ages of Gradstein et al. (1995), are listed in Table 3. As noted above, more than one biostratigraphic marker species can be used to delineate zonal or subzonal boundaries.

Methods

Calcareous nannofossils were examined using standard light microscope techniques under crossed polarizers, transmitted light, and phase contrast at 1250× magnification.

Preservation and abundance of calcareous nannofossil species may vary significantly because of etching, dissolution, or recrystallization. It is not uncommon to find specimens of nearly pristine preservation occurring in the same sample with specimens exhibiting recrystallization or etching. Thus, a simple code system to characterize preservational states has been adopted and is listed below:

VG = very good preservation: no evidence of dissolution and/or recrystallization, no alteration of primary morphologic characteristics, specimens appear diaphanous, and specimens are identifiable to the species level;
G = good preservation: little or no evidence of dissolution and/or recrystallization, primary morphologic characteristics are only slightly altered, and specimens are identifiable to the species level;
M = moderate preservation: specimens exhibit some etching and/or recrystallization, primary morphologic characteristics are somewhat altered, but most specimens are identifiable to the species level; and
P = poor preservation: specimens are severely etched or exhibit calcite overgrowth, primary morphologic characteristics are largely destroyed, fragmentation has occurred, and specimens cannot be identified at the species and/or generic level.

Six calcareous nannofossil abundance levels are recorded as follows:

D = dominant (>100 specimens per field of view);
A = abundant (10–100 specimens per field of view);
C = common (1–10 specimens per field of view);
F = frequent (1 specimen per 1–10 fields of view);
R = rare (<1 specimen per 10 fields of view); and
B = barren.

Foraminifers

Methods

Foraminifers from unlithified ooze were soaked in a 3% solution of hydrogen peroxide with a small amount of Calgon added, warmed on a hot plate, and then washed with tap water over a 63-µm sieve. Semi-lithified ooze and chalk were first partially fragmented by hand and then soaked in hydrogen peroxide and Calgon before washing. Each sieve was dipped in a dilute solution of methyl blue dye to identify contaminants from a previous sample. All samples were dried on a hot plate at ~50°C. Species identification for planktonic foraminifers were generally made on the >250-µm- and >150-µm-sized fractions, whereas two picking trays per sample from the >125-µm-sized fraction were examined for benthic foraminifer identification and abundance estimation because benthic foraminifers were rare. Samples within 0.5 m above the K/T boundary were treated the same as other unlithified ooze samples, except a 38-µm sieve was used to catch the dwarfed microfossil assemblages.

The following abundance categories were estimated from visual examination of the dried sample for planktonic foraminifers:

D = dominant (>30%);
A = abundant (10%–30%);
F = few (5%–10%);
R = rare (1%–5%); and
P = present (<1%).

Table 3. Cenozoic planktonic foraminifer datums.

Zone	Base datum marker	Base age (Ma)	Datum reference
	T *Globorotalia flexuosa*	0.07	Joyce et al., 1990
	B *Bolliella calida*	0.22	Chaproniere et al., 1994
	T *Globoquadrina pseudofoliata*	0.22	Chaproniere et al., 1994
	B *Globorotalia flexuosa*	0.40	Joyce et al., 1990
	B *Globorotalia hirsuta*	0.45	Pujol and Duprat, 1983
Pt1b	T *Globorotalia tosaensis*	0.65	Srinivasan and Sinha, 1992
	B *Globorotalia crassaformis hessi*	0.75	Chaproniere et al., 1994
	T *Pulleniatina finalis*	1.40	Chaproniere et al., 1994
Pt1a	T *Globigerinoides fistulosus*	1.77	Berggren et al., 1996
	T *Globigerinoides extremus*	1.77	Berggren et al., 1985
	Pliocene/Pleistocene boundary	1.77	
	B *Globorotalia truncatulinoides*	2.00	Zijderveld et al., 1991
	T *Globorotalia exilis* (Atlantic)	2.15	Berggren et al., 1985
Pl6	T *Globorotalia miocenica*	2.30	Berggren et al., 1996
	T *Neogloboquadrina atlantica*	2.41	Weaver and Clement, 1987
	T *Globorotalia puncticulata* (Atlantic)	2.41	Zijderveld et al., 1991
	T *Globorotalia pertenius*	2.60	Berggren et al., 1985
Pl5	T *Dentoglobigerina altispira*	3.09	Berggren et al., 1996
	T *Globorotalia multicamerata*	3.09	Berggren et al., 1985
Pl4	T *Sphaeroidinellopsis seminulina*	3.12	Berggren et al., 1996
	B *Sphaeroidinella dehiscens* sensu strictu	3.12	Weaver and Clement, 1987
	T *Globorotalia* sp. cf. *G. crassula* (N. Atlantic)	3.25	Berggren et al., 1985
	B *Globorotalia pertenuis*	3.33	Berggren et al., 1985
	Pulleniatina (disappearance in Atlantic)	3.45	Berggren et al., 1985
	B *Globorotalia miocenica* (Atlantic)	3.45	Berggren et al., 1985
Pl3	T *Globorotalia margaritae*	3.58	Berggren et al., 1996
	T *Pulleniatina primalis*	3.58	Srinivasan and Sinha, 1992
	Pulleniatina trans. sinis.-dext.	3.65	Berggren et al., 1985
	T *Pulleniatina spectabilis*	3.95	Berggren et al., 1985
Pl2	T *Globoturborotalita nepenthes*	4.18	Berggren et al., 1996
	B *Globorotalia puncticulata*	4.20	Berggren et al., 1985
	B *Globorotalia crassaformis*	4.50	Weaver and Clement, 1987
	T *Globigerinoides seiglei*	4.50	Chaproniere et al., 1994
Pl1b	T *Globorotalia cibaoensis*	4.60	Berggren et al., 1996
	B *Sphaeroidinella dehiscens* sensu lato	4.70	Berggren et al., 1985
	B *Globorotalia margaritae*	5.20	Srinivasan and Sinha, 1992
	Miocene/Pliocene boundary	5.25	
	T *Globorotalia tumida*	5.32	Srinivasan and Sinha, 1992
Pl1a	B *Globorotalia tumida*	5.60	Chaproniere et al., 1994
	B *Globorotalia sphericomiozea*	5.60	Srinivasan and Sinha, 1992
	B *Globorotalia pliozea*	5.60	Srinivasan and Sinha, 1992
	B *Globorotalia sphericomiozea*	5.60	Srinivasan and Sinha, 1992
	T *Globoquadrina dehiscens*	5.60	Chaproniere et al., 1994
M14	T *Globorotalia lenguaensis*	6.00	Chaproniere et al., 1994
	B *Globorotalia margaritae*	6.00	Chaproniere et al., 1994
	B *Neogloboquadrina acostaensis* trans. sinis.-dext.	6.00	Chaproniere et al., 1994
	B *Globorotalia margaritae*	6.20	Srinivasan and Sinha, 1992
	B *Pulleniatina primalis*	6.40	Chaproniere et al., 1994
	B *Globorotalia menardii* form 5	6.40	Chaisson and Leckie, 1993
	B *Neogloboquadrina acostaensis* trans. dext.-sinis.	6.40	Srinivasan and Sinha, 1992
	B *Neogloboquadrina atlantica* trans. dext.-sinis.	6.60	Srinivasan and Sinha, 1992
	B *Globorotalia conomiozea*	6.80	Spiegler and Jansen, 1989
	B *Globorotalia menardii* form 5	7.12	Krijgsman et al., 1994
	T *Globorotalia menardii* form 4	7.20	Krijgsman et al., 1994
	B *Globorotalia suterae*	7.40	Krijgsman et al., 1994
	B *Globorotalia cibaoensis*	7.80	Glacon et al., 1990
	B *Globorotalia juanai*	7.80	Chaisson and Leckie, 1993
	B *Candeina nitida*	8.10	Chaisson and Leckie, 1993
M13b	B *Globigerinoides extremus/Globorotalia plesiotumida*	8.30	Berggren et al., 1996
	B *Neogloboquadrina humerosa*	8.50	Berggren et al., 1985
	B *Neogloboquadrina pachyderma*	9.20	Berggren, 1992
	T *Neogloboquadrina nympha*	10.10	Berggren, 1992
M13	B *Neogloboquadrina acostaensis*	10.90	Berggren et al., 1996
	B *Neogloboquadrina acostaensis*	10.90	Miller et al., 1991
M12	T *Neogloboquadrina mayeri*	11.40	Miller et al., 1994
M11	B *Globoturborotalita nepenthes*	11.80	Miller et al., 1994
	T *Globorotalia panda*	11.80	Berggren, 1993
M10	T *Globorotalia fohsi robusta*	11.90	Berggren et al., 1985
	T *Globorotalia praescitula*	11.90	Berggren, 1992
	T *Globorotalia fohsi lobata*	12.10	Wright and Miller, 1992
M9b	B *Globorotalia foshi robusta*	12.30	Berggren, 1992
	T *Tenuitella clemenciae*	12.30	Li et al., 1992
	T *Tenuitella minutissima*	12.30	Li et al., 1992
	T *Tenuitella pseudoedita*	12.30	Li et al., 1992
	T *Tenuitella selleyi*	12.30	Li et al., 1992
M9a	B *Globorotalia fohsi lobata*	12.50	Wright and Miller, 1992
M8	B *Globorotalia fohsi* sensu stricto	12.70	Wright and Miller, 1992
	B *Globorotalia praefohsi*	12.70	Wright and Miller, 1992
	B *Neogloboquadrina nympha*	13.40	Berggren, 1992
	T *Globorotalia peripheroronda*	14.60	Berggren et al., 1985
M7	B *Globorotalia peripheroacuta*	14.80	Berggren et al., 1996
	T *Praeorbulina sicana*	14.80	Berggren et al., 1985
	T *Praeorbulina glomerosa* sensu stricto	14.80	Berggren et al., 1985
M6	B *Orbulina suturalis*	15.10	Berggren et al., 1985
	T *Globorotalia miozea*	15.90	Berggren, 1992
	B *Praeorbulina circularis*	16.00	Berggren et al., 1985
M5b	B *Praeorbulina glomerosa*	16.10	Berggren et al., 1996

Table 3 (continued).

Zone	Base datum marker	Base age (Ma)	Datum reference
	B *Globigerinoides diminutus*	16.10	Berggren et al., 1985
	B *Praeorbulina curva*	16.30	Berggren et al., 1985
M5	B *Praeorbulina sicana*	16.40	Berggren et al., 1985
	T *Globorotalia incognita*	16.40	Berggren, 1992
M4b	B *Globorotalia birnageae*	16.70	Berggren et al., 1996
	B *Globorotalia miozea*	16.70	Berggren, 1992
	B *Globorotalia birnageae*	16.70	Berggren et al., 1985
M4	T *Catapsydrax dissimilis*	17.30	Berggren et al., 1985
	T *Globorotalia zealandica*	17.30	Li et al., 1992
	T *Globorotalia semivera*	17.30	Berggren et al., 1985
	T *Globoquadrina dehiscens* forma *spinosa*	17.90	Berggren et al., 1985
	B *Globorotalia praescitula*	18.50	Miller et al., 1994
M3	B *Globorotalia insueta*	18.80	Berggren et al., 1996
	B *Globigerinoides altiaperturus*	20.50	Montanari et al., 1991
	T *Tenuitella munda*	21.40	Li et al., 1992
M2	T *Globorotalia kugleri*	21.50	Montanari et al., 1991
	B *Globorotalia incognita*	21.60	Berggren, 1992
	T *Globoturborotalita angulisuturalis*	21.60	Berggren et al., 1985
	T *Globorotalia pseudokugleri*	21.60	Berggren et al., 1985
	B *Globoquadrina dehiscens* forma *spinosa*	22.20	Berggren et al., 1985
	T *Globoquadrina globularis*	22.80	Berggren et al., 1985
M1b	B *Globoquadrina dehiscens*	23.20	Berggren et al., 1985
M1	B *Globorotalia kugleri*	23.80	Berggren et al., 1985
	B *Globorotalia mendacis*	23.80	Berggren et al., 1985
	Oligocene/Miocene boundary	23.80	
	T *Globigerina euapertura*	23.80	Berggren, 1992
	T *Tenuitella gemma*	24.30	Li et al., 1992
	FCO *Globigerinoides primordius*	24.30	Berggren et al., 1985
	B *Globorotalia pseudokugleri*	25.90	Leckie et al., 1993
	B *Globigerinoides primordius*	26.70	Leckie et al., 1993
P22	T *Paragloborotalia opima opima*	27.10	Berggren et al., 1985
	T *Globigerina labiacrassata*	27.10	Berggren, 1992
P21b	LCO *Chiloguembelina cubensis*	28.50	Li et al., 1992
P21	B *Globigerina angulisuturalis*	28.50	Blow, 1969
	B *Globigerinita boweni*	28.50	Li et al., 1992
P21a	B *Globigerina angulisuturalis*	29.40	Leckie et al., 1993
	B *Tenuitellinata juvenilis*	29.70	Li et al., 1992
	T *Subbotina angiporoides*	30.00	Berggren, 1992
P20	T *Turborotalia ampliapertura*	30.30	Miller et al., 1993
	B *Paragloborotalia opima opima*	30.60	Berggren et al., 1985
P19	T *Pseudohastigerina* spp.	32.00	Miller et al., 1993
	B *Cassigerinella chipolensis*	33.65	Miller et al., 1993
	Eocene/Oligocene boundary	33.70	
	T *Hantkenina* spp.	33.70	Coccioni et al., 1988
P18	T *Turborotalia cerroazulensis*	33.80	Coccioni et al., 1988
P17	T *Cribrohantkenina inflata*	34.00	Coccioni et al., 1988
	T *Globigerapsis index*	34.30	Berggren, 1992
P16	B *Turborotalia cunialensis*	35.20	Coccioni et al., 1988
	T *Turborotalia pomeroli*	35.30	Premoli-Silva et al., 1988
	T *Porticulasphaera semiinvoluta*	35.30	Premoli-Silva et al., 1988
	B *Cribrohantkenina inflata*	35.50	Coccioni et al., 1988
	T *Acarinina* spp.	37.50-38.50	Nocchi et al., 1986
	T *Acarinina collactea*	37.70	Berggren et al., 1985
	T *Subbotina linaperta*	37.70	Berggren, 1992
	T *Morozovella spinulosa*	38.10	Berggren et al., 1985
P15	B *Porticulasphaera semiinvoluta*	38.40	Nocchi et al., 1986
	T *Planorotalites* spp.	38.50	Nocchi et al., 1986
	T *Acarinina primitiva*	39.00	Stott and Kennett, 1990
	T *Subbotina frontosa*	39.30	Berggren et al., 1985
P14	T *Globigerinapsis beckmanni*	40.10	Berggren et al., 1986
P13	B *Globigerinapsis beckmanni*	40.50	Berggren et al., 1987
	T *Acarinina bullbrooki*	40.50	Berggren et al., 1988
	B *Turborotalia pomeroli*	42.40	Berggren et al., 1989
	T *Globigerapsis index*	42.90	Berggren et al., 1990
	B *Morozovella lehneri*	43.50	Berggren et al., 1991
P12	T *Morozovella aragonensis*	43.60	Berggren et al., 1992
P11	B *Globigerinapsis kugleri*	45.80	Berggren et al., 1996
	B *Turborotalia possagnoensis*	46.00	Berggren et al., 1995
P10	B *Hantkenina nutalli*	49.00	Berggren et al., 1985
P9	B *Planorotalites palmerae*	50.40	Berggren et al., 1985
P8	T *Morozovella formosa*	50.80	Berggren, 1969
	B *Acarinina pentacamerata*	50.80	Stott and Kennett, 1990
P7	B *Morozovella aragonensis*	52.30	Berggren et al., 1995
	T *Morozovella marginodentata*	52.50	Berggren et al., 1995
	T *Morozovella lensiformis*	52.70	Berggren et al., 1995
	T *Subbotina velascoensis*	53.50	Berggren et al., 1995
	T *Morozovella aequa*	53.60	Berggren et al., 1995
P6b	B *Morozovella f. formosa/Morozovella lensiformis*	54.00	Berggren and Miller, 1988
	B *Morozovella lensiformis*	54.00	Berggren et al., 1995
P6	T *Morozovella velascoensis*	54.70	Berggren et al., 1995
	Paleocene/Eocene boundary	54.70	
	T *Morozovella acuta*	54.70	Berggren et al., 1995
	B *Morozovella formosa gracilis*	54.70	Berggren et al., 1995
	B *Igorina broedermanni*	54.70	Berggren et al., 1995
	B *Morozovella marginodentata*	54.80	Berggren et al., 1995
	B *Globanomalina australiformis*	55.50	Berggren et al., 1995
	B *Globanomalina australiformis*	55.50	Stott and Kennett, 1990

Table 3 (continued).

Zone	Base datum marker	Base age (Ma)	Datum reference
	T *Morozovella acuta*	55.70	Berggren et al., 1995
P5	T *Globanomalina pseudomenardii*	55.90	Berggren et al., 1995
	T *Acarinina mckannai*	56.30	Berggren et al., 1995
	T *Acarinina acarinata*	56.30	Berggren et al., 1995
P4c	B *Acarinina soldadoensis*	56.50	Berggren et al., 1995
	B *Acarinina coalingensis*	56.50	Berggren et al., 1995
	B *Morozovella aequa*	56.50	Berggren et al., 1995
	B *Morozovella subbotinae*	56.90	Berggren et al., 1995
P4b	T *Acarinina subsphaerica*	57.10	Berggren et al., 1995
	B *Acarinina mckannai*	59.10	Berggren et al., 1995
P4a	B *Globanomalina pseudomenardii*	59.20	Berggren et al., 1996
	T *Parasubbotina variospira*	59.20	Berggren et al., 1995
	T *Parasubbotina varianta*	59.20	Berggren et al., 1995
	B *Acarinina acarinata*	59.20	Berggren et al., 1995
	B *Acarinina subsphaerica*	59.20	Berggren et al., 1995
P3b	B *Igorina albeari*	60.00	Berggren et al., 1995
	B *Morozovella velascoensis*	60.00	Berggren et al., 1995
	B *Praemurica strabocella*	60.50	Berggren et al., 1995
	B *Morozovella conicotruncata*	60.90	Berggren et al., 1995
P3a	B *Morozovella angulata*	61.00	Berggren et al., 1996
	B *Igorina pusilla*	61.00	Berggren et al., 1995
P2	B *Praemurica uncinata*	61.20	Berggren et al., 1995
	B *Morozovella praeangulata*	61.20	Berggren et al., 1995
	B *Globanomalina imitata*	61.30	Berggren et al., 1995
P1c	B *Globanomalina compressa/Praemurica inconstans*	63.00	Berggren et al., 1996
	B *Parasubbotina varianta*	63.00	Berggren et al., 1995
	B *Praemurica inconstans*	63.00	Berggren et al., 1995
P1b	B *Subbotina triloculinoides*	64.50	Berggren et al., 1995
P1a	T *Parvularugoglobigerina eugubina*	64.90	Berggren et al., 1995
Pα	B *Parvularugoglobigerina eugubina*	64.97	Berggren et al., 1995
P0	T *Globotruncana*	65.00	Berggren et al., 1995

Notes: T = top; B = bottom; FCO = first common occurrence; LCO = last common occurrence; trans. sinis.-dext. = sinistral-dextral. For datum references, see Berggren et al. (1995).

Table 4. Cretaceous planktonic foraminifer zones and datums.

Zone name	Base event	Zone author	Date	Age (Ma)
Abathomphalus mayaroensis	FO *A. mayaroensis*	Brönnimann	1952	68.3
Racemiguembelina fructicosa	FO *R. fructicosa*	Smith and Pessagno	1973	69.6
	FO *C. contusa*			69.6
Gansserina gansseri	FO *G. gansseri*	Brönnimann	1952	72.8
Globotruncana falsostuarti	LO *R. calcarata*	Salaj and Samuel	1966	75.2
Radotruncana calcarata	FO *R. calcarata*	Herm	1962	75.7
Globotruncana ventricosa	FO *G. ventricosa*	Dalbiez	1955	79.5
Globotruncanita elevata	LO *D. asymetrica*	Dalbiez	1955	83.2
Dicarinella asymetrica	FO *D. asymetrica*	Postuma	1971	85.4
Dicarinella concavata	FO *D. concavata*	Sigal	1955	89.7
Marginotruncana schneegansi	LO *H. helvetica*	Bolli	1966	90.8
Helvetoglobotruncana helvetica	FO *H. helvetica*	Dalbiez	1955	93.1
Whiteinella archaeocretacea	LO *R. cushmani*	Bolli	1966	93.9
Rotalipora cushmani	FO *R. cushmani*	Borsetti	1962	96.6
Rotalipora reicheli	FO *R. reicheli*	Bolli	1966	96.9
Rotalipora greenhornensis	FO *R.greenhornensis*	Lehmann	1966	98.9
Rotalipora appenninica	FO *R. appenninica*	Bolli	1966	100.4
Rotalipora ticinensis	FO *R. ticinensis*	Dalbiez	1955	101.8
Rotalipora subticinensis	FO *R. subticinensis*	Postuma	1971	102.5
Ticinella praeticinensis	FO *T. praeticinensis*	Moullade	1966	105.0
Ticinella primula	FO *T. primula*	Moullade	1966	109.0
Hedbergella planispira	LO *T. bejaouaensis*	Moullade	1966	112.5
Ticinella bejaouaensis	FO *T. bejaouaensis*	Moullade	1966	114.0
Hedbergella gorbachikae	LO *G. algerianus*	Longoria	1974	115.0
Globigerinelloides algerianus	FO *G. algerianus*	Moullade	1966	116.9
Globigerinelloides ferreolensis	LO *L. cabri*	Moullade	1966	118.0
Leupoldina cabri	FO *L. cabri*	Bolli	1959	119.0
Globigerinelloides blowi	FO *G. blowi*	Moullade	1974	123.9
Globigerinelloides duboisi	FO *G. duboisi*	Sigal	1977	

Notes: FO = first occurrence; LO = last occurrence. See Caron (1985) for zone author bibliography. Datum ages are from Erba et al. (1995).

The following abundance categories were used for benthic foraminifer abundance (as a group), based on the number of benthic foraminifers encountered in two picking trays:

A = abundant (>100 specimens);
C = common (50–100 specimens);
F = few (20–50 specimens);
R = rare (10–20 specimens); and
T = trace (<10 specimens).

The preservation status of the planktonic and benthic foraminifers is estimated as follows:

VG (very good) = no evidence of overgrowth, dissolution, or abrasion;
G (good) = little evidence of overgrowth, dissolution, or abrasion;

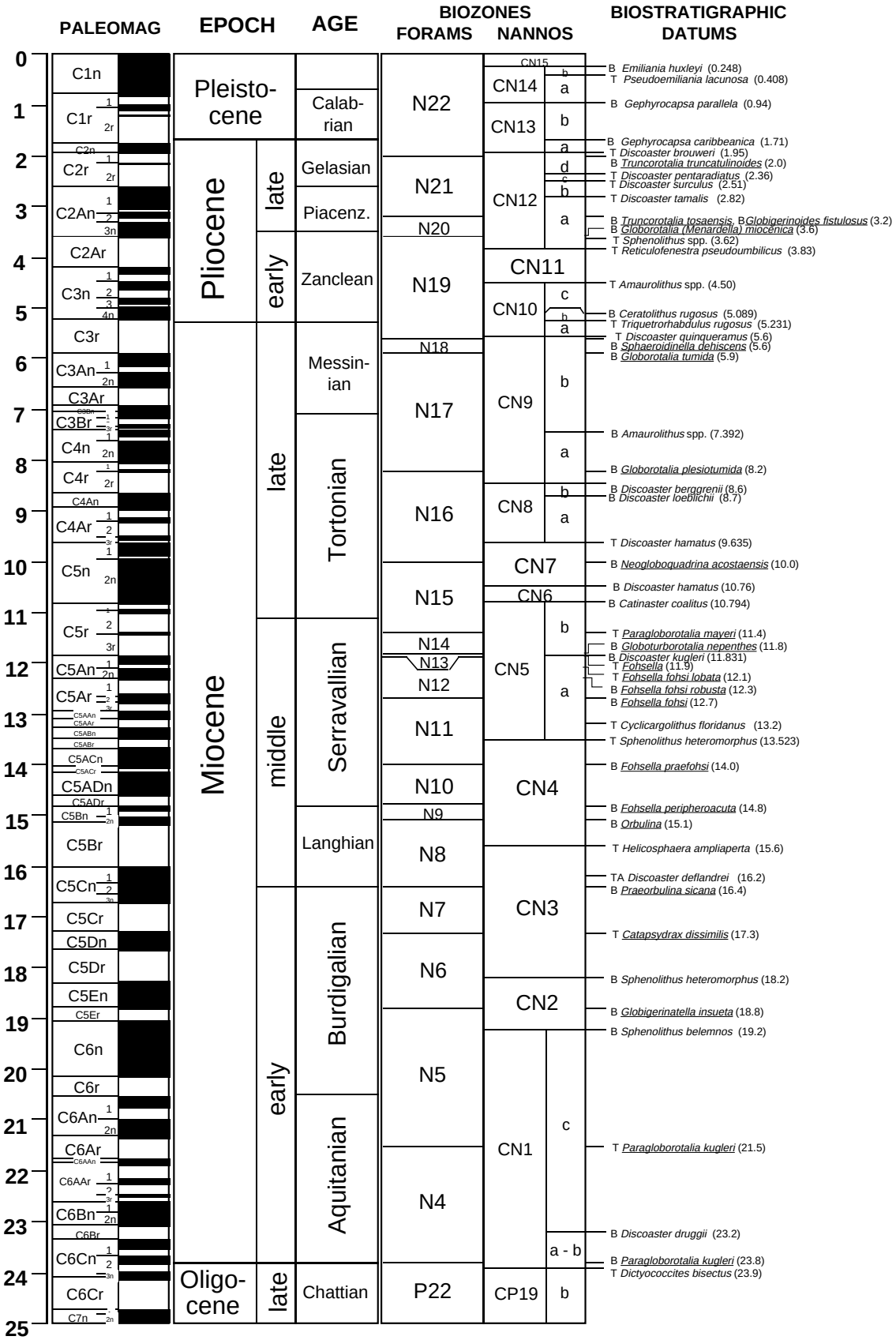

Figure 5. Leg 171B correlation chart.

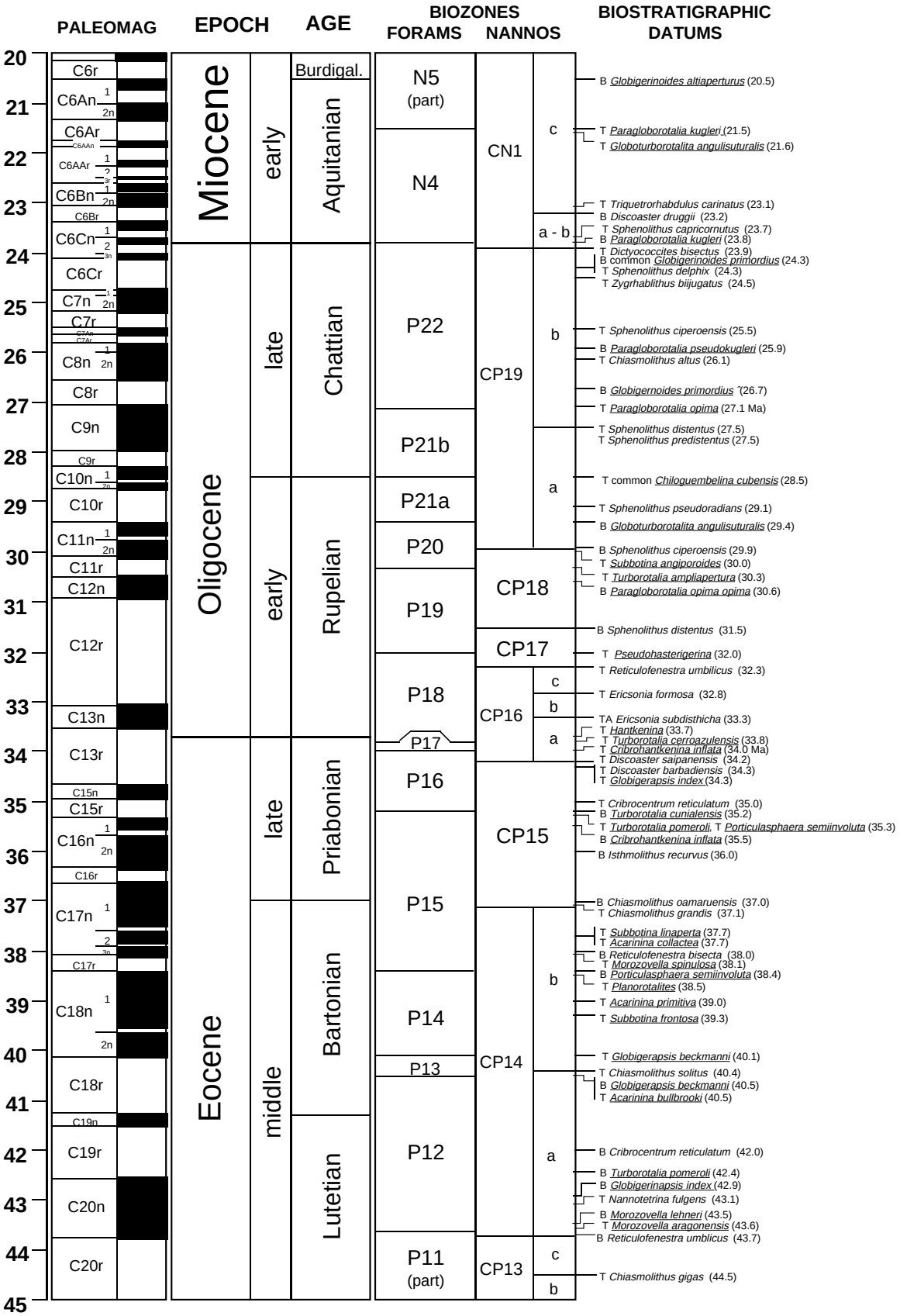

Figure 5 (continued).

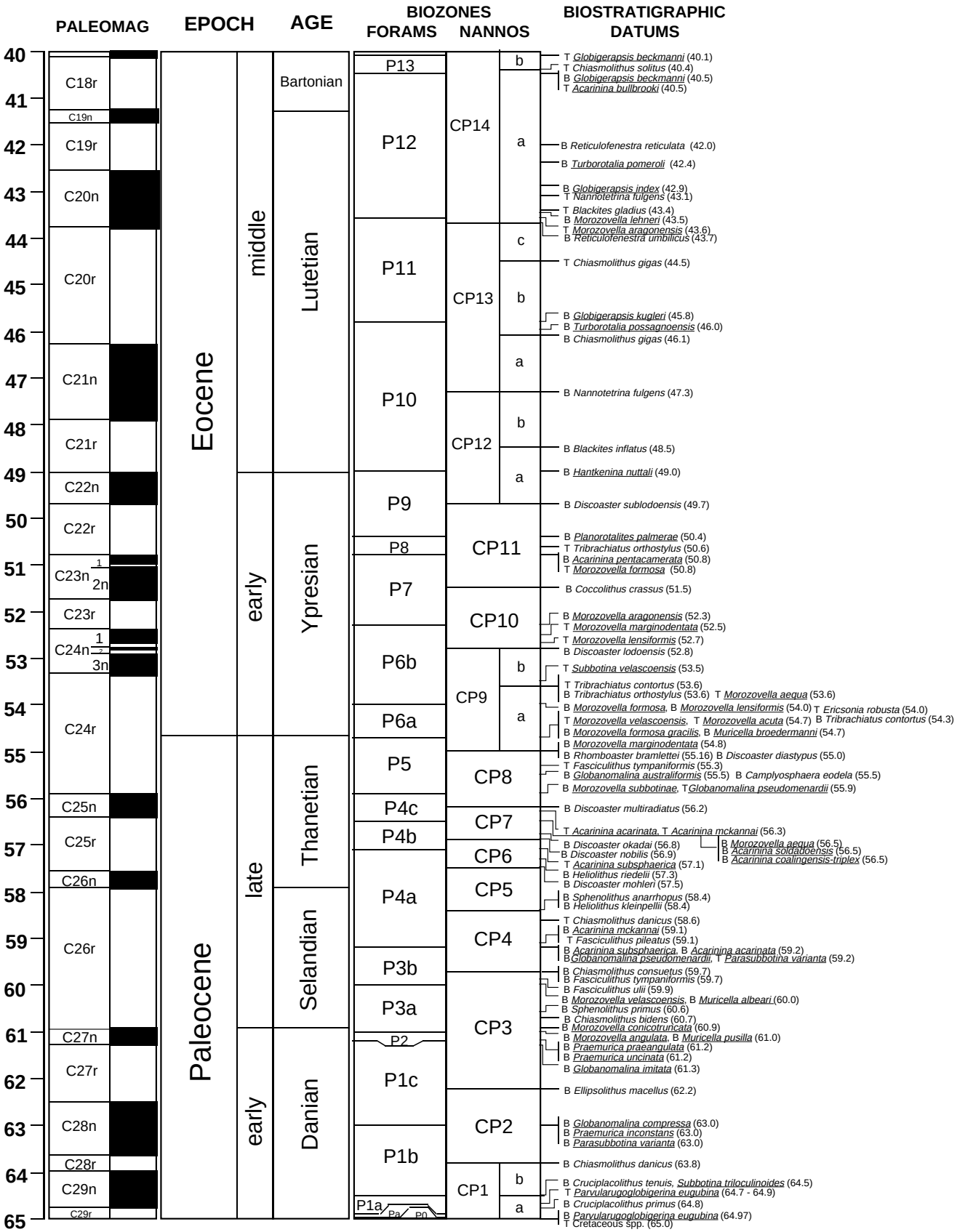

Figure 5 (continued).

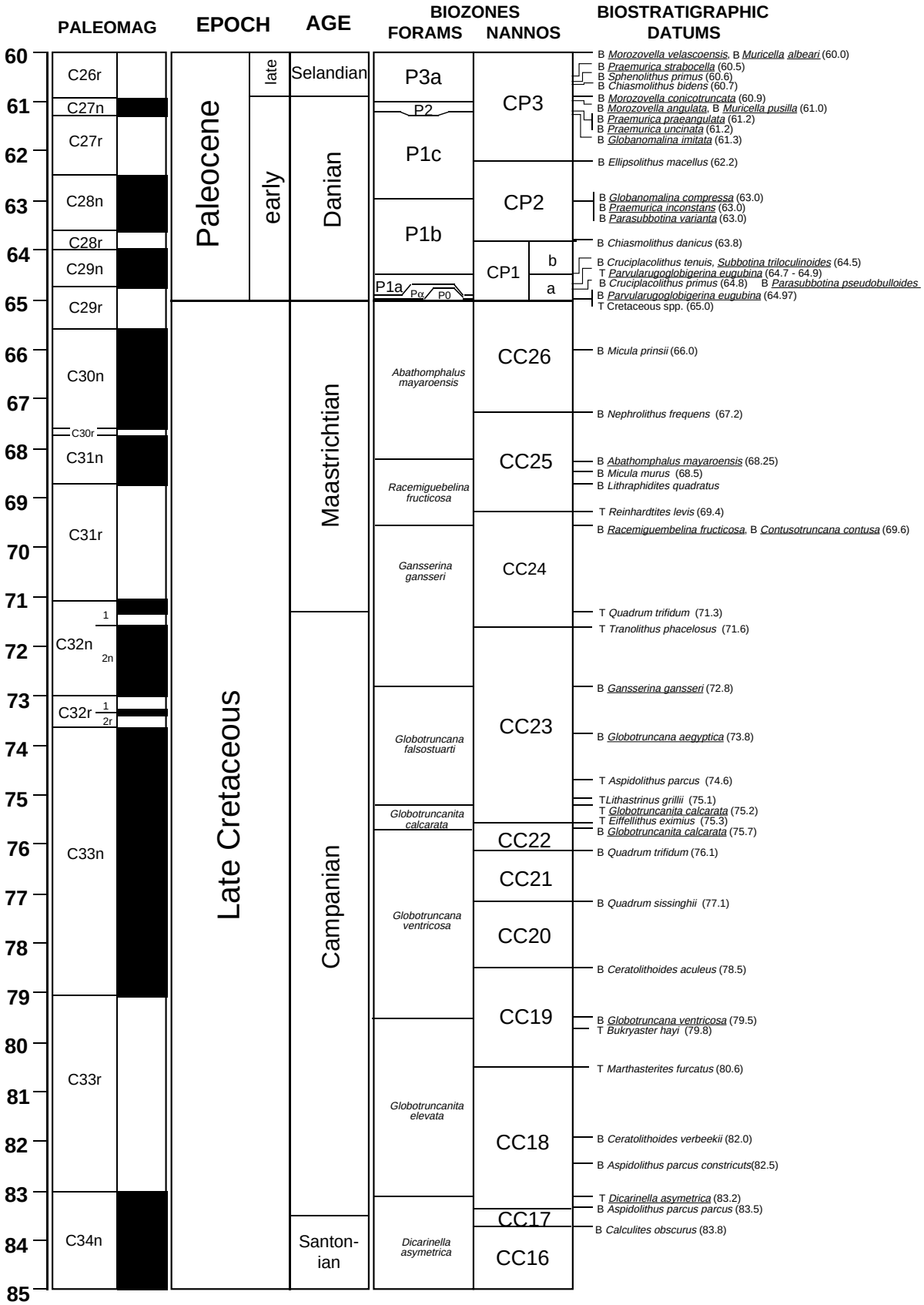

Figure 5 (continued).

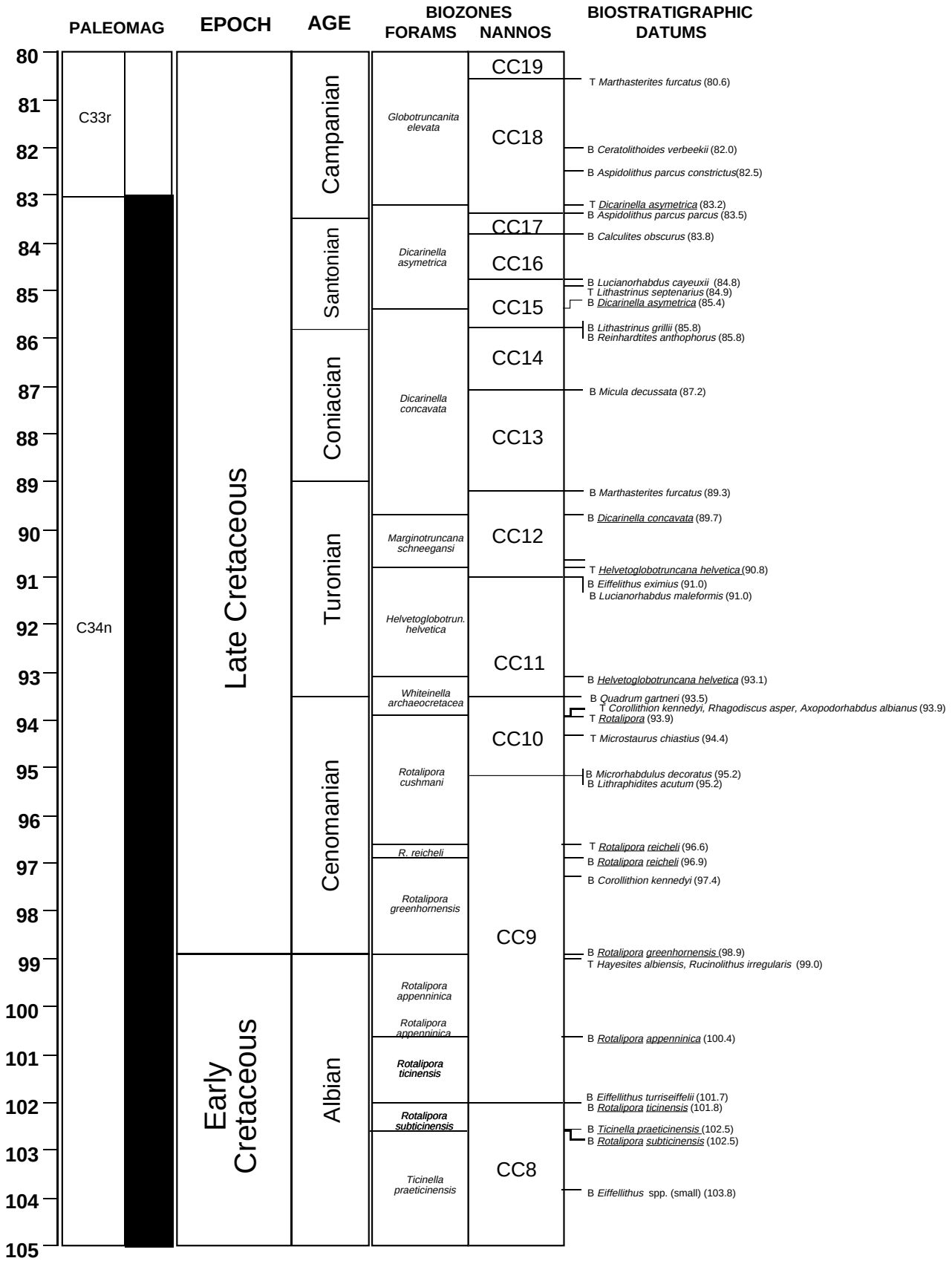

Figure 5 (continued).

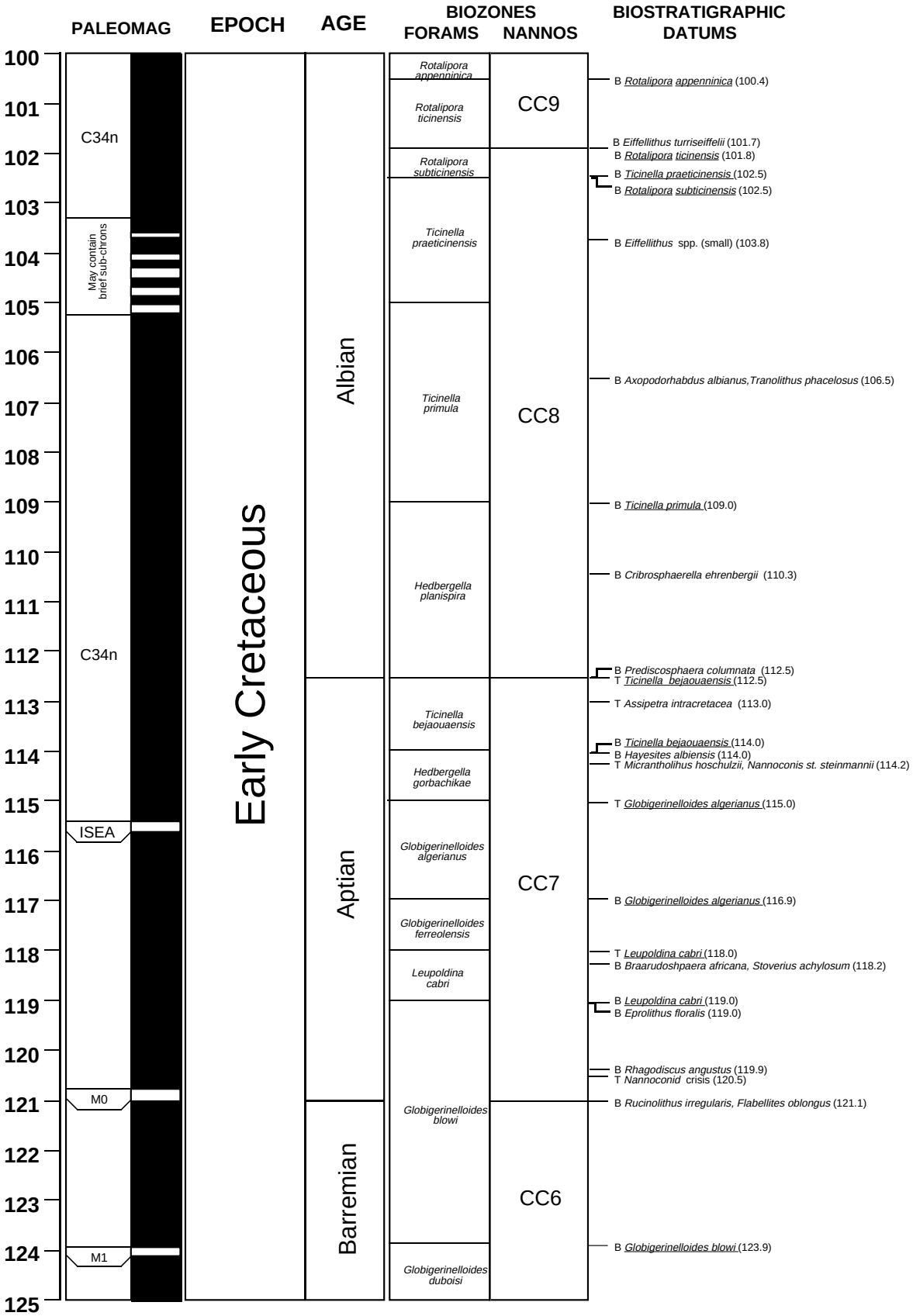

Figure 5 (continued).

M (moderate) = calcite overgrowth, dissolution, or abrasion are common but minor; and
P (poor) = substantial overgrowth, dissolution, or fragmentation.

Planktonic Foraminifer Taxonomy

Cenozoic taxonomic concepts follow Kennett and Srinivasan (1983) and Chaisson and Leckie (1993) for the Neogene, Toumarkine and Luterbacher (1985) for the Eocene and Oligocene, and Olsson et al. (in press) for the Paleocene. Genus-species combinations generally follow those used by Berggren et al. (1995). Cretaceous taxonomic concepts are based on Robaszynski and Caron (1979), Robaszynski et al. (1984), and Bellier (1983); trochospiral taxa are based on Caron (1985); and serial taxa are based on Nederbragt (1991).

Planktonic Foraminifer Zonal Scheme and Datums

The tropical planktonic foraminifer zonal scheme for the Cenozoic and ages for the Cenozoic datums follow Berggren et al. (1995). These are presented in Figure 5 and Table 3. The zonation used for Cretaceous planktonic foraminifers is based on the tropical zonal scheme of Caron (1985), with some modifications (Fig. 6). The authors responsible for defining the bases of the Cretaceous zones are listed in Table 3, and age estimates for planktonic foraminifer datum markers were obtained from Erba et al. (1995).

Benthic Foraminifer Taxonomy

Cenozoic taxonomic concepts were based mainly on Van Morkhoven et al. (1986) and Tjalsma and Lohmann (1983). Upper Cretaceous taxonomic concepts follow Widmark (1997), and for identifications of the Lower Cretaceous benthic foraminifers, Gradstein (1978) and Basov and Krasheninnikov (1983) were used.

Radiolarians

Zonation

Correlation of radiolarian zones follows Berggren and Miller (1988) and Barron (1989) for the Oligocene; Aubry et al. (1988) for the Eocene and Paleocene. During Leg 171B, the low-latitude zonal schemes of Riedel and Sanfilippo (1978), Sanfilippo et al. (1985), and Bolli et al. (1985) were used for the Cenozoic sediments. The numbers R1 through R16 were assigned to Leg 171B radiolarian zonal schemes (Riedel and Sanfilippo, 1978; Fig. 6). The standard zonation used for Cretaceous sediments was that of Sanfilippo and Riedel (1985). However, additional zonal schemes had to be used for age determination, including those of Foreman (1968; latest Cretaceous and earliest Paleocene), Hollis (1993; K/T boundary faunas), Jud (1994; Lower Cretaceous), O'Dougherty (1994; mid-Cretaceous), Pessagno (1976; Upper Cretaceous), Pessagno (1977; Lower Cretaceous), and Schaaf (1981, 1984; Lower Cretaceous).

Abundance and Preservation

Radiolarian abundance data discussed in the "Biostratigraphy" sections of the site chapters (this volume) were based on strewn- or dry-picked slides of sieved acid residues. Consequently, some observations may differ markedly from the lithologic descriptions, which were described on the basis of raw smear-slide data. Abundance estimates are qualitative and were determined by visual approximation of the total number of specimens observed per microscope traverse. The radiolarian abundances have the following range of absolute frequency (specimens per traverse):

A (abundant) = >100 specimens per traverse;
C (common) = 51–100 specimens per traverse;

EPOCH	LOW LATITUDE PALEOGENE RADIOLARIAN ZONES	ZONE NUMBER
Oligocene	*Dorcadospyris ateuchus*	R16
	Theocyrtis tuberosa	R15
late Eocene	*Cryptocarpium ornatum*	R14
	Calocyclas bandyca	R13
	Cryptocarpium azyx	R12
middle Eocene	*Podocyrtis goetheana*	R11
	Podocyrtis chalara	R10
	Podocyrtis mitra	R9
	Podocyrtis ampla	R8
	Thyrsocyrtis triacantha	R7
	Dictyoprora mongolfieri	R6
	Thyecotyle cryptocephala	R5
early Eocene	*Phormocyrtis striata striata*	R4
	Buryella clinata	R3
Paleocene	*Bekoma bidartensis*	R2
	Bekoma campechensis	R1

Figure 6. Leg 171B radiolarian zonation chart.

F (few) = 11–50 specimens per traverse;
R (rare) = 1–10 specimens per traverse;
T (trace) = <1 specimen per traverse or a few fragments; and
B (barren) = no radiolarian skeletons or fragments.

Degraded preservation was largely the result of dissolution effects. The preservation of skeletons was noted as

VG (very good) = nearly all of the specimens observed were complete, with spines intact and no overgrowths;
G (good) = a majority of specimens were not broken, corroded, or recrystallized;
M (moderate) = a substantial portion of the specimens were broken, and some degree of overgrowth or etching was observed; and
P (poor) = specimens were mostly broken and fragmentary and showed substantial overgrowth.

Sample Preparation

Most of the radiolarian slides were prepared by submersing the sample in hot water containing a small amount of Calgon and then treating the sample with a 15% HCl solution until the calcareous component was removed. Additionally, boiling the sample in 20% hydrogen peroxide for 3–5 min was necessary if the sample was indurated. The sample was then sieved using 80- and 230-mesh (180- and 63-µm) stainless-steel sieves. If the sediment did not fully disaggregate, the procedure was repeated. Ultrasound was used sparingly (5-s intervals) and only when chemical processing did not completely disaggregate the clay component. After processing, the >63-µm fraction was strewn on slides, covered with Piccolyte, and protected with a glass cover 22 mm × 40 mm in size.

The Cenozoic samples were examined by standard transmitted-light techniques, but the Mesozoic samples were first examined in water using reflected-light microscopy to determine if any radiolarians were present. Reflected-light microscopy was used to study Mesozoic faunas because the skeletons had been recrystallized to quartz.

PALEOMAGNETISM

Paleomagnetic studies performed aboard the *JOIDES Resolution* during Leg 171B included routine measurements of natural remanent magnetization (NRM). The measurement of magnetic remanence was generally accompanied by alternating-field (AF) demagnetization to remove secondary magnetizations. Shipboard analysis of continuous half-core sections were supplemented by progressive thermal demagnetization of 1000 discrete minicores, using paleomagnetic laboratories at the University of Oxford and the University of Michigan. For each hole, tabulated paleomagnetic measurements for each discrete sample (in tab-delimited ASCII format) and a summary of the preliminary polarity interpretations with graphical representations (in PDF format) are included on CD-ROM (back pocket, this volume).

Shipboard Laboratory Facilities

The paleomagnetic laboratory on the *JOIDES Resolution* is equipped with two magnetometers: a pass-through cryogenic superconducting direct current–superconducting quantum interference device rock magnetometer, manufactured by 2-G Enterprises (model 760R), and a Molspin spinner magnetometer. An in-line AF demagnetizer, capable of 80 mT (2-G model 2G600), is included on the pass-through cryogenic magnetometer track for the demagnetization of continuous sections. The sensing coils in the cryogenic magnetometer measure the magnetic signal over about a 10-cm interval, and the coils for each axis have slightly different response curves. The widths of the sensing regions correspond to about 100–150 cm^3 of cored material, all of which contribute to the signal at the sensors. The large volume of core material within the sensing region allows the accurate determination of remanence for weakly magnetized samples, despite the relatively high background noise related to the motion of the ship. The practical limit on the resolution of the natural remanence of the core samples is usually imposed by the magnetization of the core liner itself, which is ~0.01 mA/m (10^{-8} emu/cm^3).

For the demagnetization of discrete samples, the laboratory contains a thermal demagnetizer and an AF demagnetizer (Schonstedt Instrument Co., models TSD-1 and GSD-1, respectively) capable of demagnetizing discrete specimens to 700°C and 100 mT, respectively. Partial anhysteretic remanent magnetization (pARM) can be imparted to discrete samples by a DTECH, Inc., pARM-2 system. This double-coil system is used in conjunction with the GSD-1 demagnetizer to apply a bias field to a sample during AF demagnetization; the bias field can be switched on optionally only over a window of AF field intensity during the declining-field stage of the demagnetization cycle. All demagnetization devices and magnetometers are shielded within µ-metal cylinders. An Analytical Services Company (ASC) model IM-10 impulse magnetizer is also available for studies of the acquisition of both stepwise and saturation isothermal remanence magnetization (IRM) by discrete samples. This unit can apply pulsed fields from 20 to 1200 mT. Anisotropy of magnetic susceptibility (AMS) can be measured on board the ship using a KLY-2 Kappabridge magnetic susceptibility bridge, which has a sensitivity of 1×10^{-6} (SI volume units).

Remanent Magnetization Measurements

Remanence measurements were performed by passing continuous archive-half-core sections through the cryogenic magnetometer. The ODP core orientation scheme arbitrarily designates the positive x-axis direction as the horizontal (in situ) direction from the center of the core to the median line between a pair of lines inscribed lengthwise on the working half of each core liner (Fig. 7). The NRM and remanence measurements after AF demagnetization of 5, 19, 15, and/or 20 mT were routinely measured at 3- to 10-cm intervals. At least one discrete sample was taken from each section for progressive thermal or AF demagnetization in shore-based laboratories to characterize the magnetic behavior and to verify polarity interpretations. Discrete minicore samples were taken from soft sediment using oriented plastic cylinders (10 cm^3), followed by extrusion and trimming, or were drilled from lithified sedimentary rocks using a water-cooled nonmagnetic drill bit attached to a standard drill press. Whole-core susceptibility measurements provide an indication of the amount of magnetic material in the sediment. These measurements were performed using the multisensor track (MST; see "Physical Properties" section, this chapter). Susceptibility was also measured on all discrete samples before and after the suite of thermal demagnetizations.

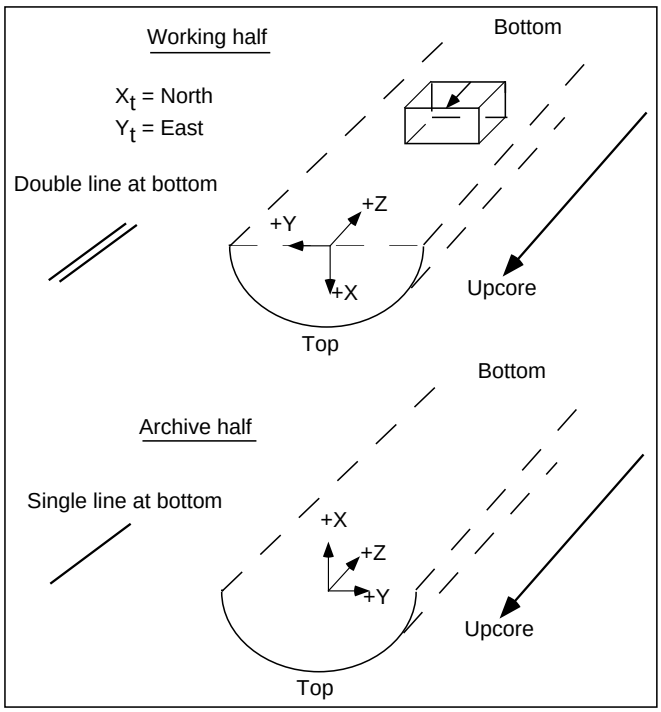

Figure 7. Core orientation convention for split-core sections and discrete samples.

Core Orientation

Orientation of cores recovered with the advanced hydraulic piston (APC) corer was achieved with a tensor tool mounted on the core barrel. The tensor tool consists of a three-component fluxgate magnetometer and a three-component accelerometer, rigidly attached to the core barrel. The information from both sets of sensors allows the azimuth and dip of the hole to be measured as well as the azimuth of the double orientation line on the core liner. Orientation is not usually attempted for the top three cores (to about 30 meters below seafloor [mbsf]), until the bottom-hole assembly (BHA) is sufficiently stabilized in the sediment. Core orientation by the tensor tool was relative to magnetic north.

Reorientation of the rotated portions of cores recovered with the rotary core barrel (RCB) and extended core barrel (XCB) devices can be accomplished by using paleomagnetic results. Discrete samples were thermal or AF demagnetized, and the characteristic remanence direction was calculated using a three-dimensional mean vector fit to selected intervals of the demagnetization curve. Following any correction for bedding tilt, the declinations of the characteristic directions were then rotated to 0° for normal polarity or to 180° for reversed polarity.

Magnetostratigraphy

Where magnetic cleaning successfully isolates the primary component of remanence, the polarity is interpreted from the clustering of positive (downward, hence normal polarity) or from negative (upward, hence reversed polarity) paleomagnetic inclinations. Declinations relative to magnetic north derived from the tensor tool aided in assigning a magnetic polarity to the stratigraphic columns in APC intervals. Interpretations of the magnetic polarity stratigraphy, with constraints from the biostratigraphic data, are presented in the site chapters. The revised time scale of Cande and Kent (1995; see Table 5) was used for Cenozoic polarity boundaries, and the time scale of Gradstein et al. (1995; see Table 5) was used for Cretaceous polarity boundaries.

CORE-CORE INTEGRATION

Several of the scientific objectives of Leg 171B require examination of the sedimentary records at high resolution; this, in turn, demands attention to the completeness of the recovered sections that has in the past normally been devoted only to Pleistocene sections. To achieve this, we used the strategy pioneered by Hagelberg et al. (1992) during Leg 138. Hagelberg et al. utilized high-resolution density data obtained with the gamma-ray attenuation porosity evaluator (GRAPE) and magnetic susceptibility and digital reflectance data to document the exact correlation among cores at each of the several holes at a particular site. Inevitably, this necessitates depth shifting each core to align features that are obviously correlative. Material is commonly found to be missing between successive cores in each hole, even where there is nominal 100% recovery. The end product of this depth shifting is a new depth scale (m composite depth [mcd]) that has the advantage of representing continuity but the disadvantage of being longer than the distance actually cored (mbsf). Typically, the length is expanded by about 10%, but the factor varies between about 5% and 15%. The reason for this expansion is not fully understood, but certainly both decompression of the sediment (Moran, 1997) and distortion by the coring process are involved. To maintain a linear relationship between mcd and curated depths within a single core, it is highly desirable to apply a single depth offset to an entire 9.5-m core.

To obtain a meaningful representation of the whole section recovered, it is convenient to create a spliced record (Hagelberg et al., 1992) that is constructed by adding sequential intervals of core from any of the holes recovered, proceeding down from the seafloor. Such a splice is useful both for providing a continuous record of the shipboard high-resolution records for time-series analysis and a template for sampling the complete section for shore-based analysis without wasting sediment samples or analytical time.

A significant limitation of this approach is that, because of drilling-induced distortion, it is seldom possible to line up all the prominent features in two cores by using a linear depth offset. It is convenient to align two cores at their crossover point when compiling the splice. If the relationship between samples in parallel holes must be known precisely, it may be necessary post cruise to map the data for each section of each hole into the splice, thereby creating another depth scale that is not linearly related to curated depth at the centimeter to decimeter scale (Hagelberg et al., 1995). Such a scale should be used only for special purposes, and great caution is required to avoid generating unnecessary confusion.

During Leg 171B, the core-core integration was performed using SPLICER, a software package developed by Peter deMenocal and Ann Esmay of the Lamont-Doherty Earth Observatory Borehole Research Group (LDEO-BRG). The data sets used were MST magnetic susceptibility and GRAPE density data and output from the Minolta color scanner. However, unlike previous users, we made use of the L*a*b output from the Minolta instead of the reflectance from individual color channels. In some core sections, changes in lightness (i.e., generalized reflectance) are useful for correlation, but elsewhere it is color, rather than lightness, that is useful. Thus, the L*a*b output provides better information. The Munsell code output would be equally appropriate, but it is not conveniently processed by the SPLICER software.

The use of a composite depth section significantly improves the ability to describe changes in the sedimentation rate, especially if biostratigraphy and magnetostratigraphy provide a dense network of precisely determined age-control points. The sedimentation rates (mcd/m.y.) are artificially high, by about 10%, as a consequence of the stretched mcd scale; post-cruise alignment of MST data with the downhole logs may enable us to adjust the mcd depth scale to logging depths. Note that to the extent that expansion caused by rebound can explain the growth of the mcd depth scale, mass fluxes would be correct when calculated using densities measured aboard ship and sedimentation rates calculated using the mcd scale. The reason for this is that the mechanism envisages the sediment expanding during rebound by an increase in porosity. In reality, sediment fluxes on geologic time scales can rarely—perhaps never—be specified with sufficient precision that the difference between the mcd and mbsf scales is a significant concern. It is, however, important for some applications to rescale depth on the mcd scale back to the true depth below seafloor. For example, to simulate a seismic section using physical properties measured in core, it is vital to use the composite depth splice to simulate the complete section. On the other hand, the simulation must be rescaled to true depth to correctly predict the depths of reflectors in the subsea sediment. Rescaling can be done most simply by a linear transformation based on the ratio of mcd to mbsf over the full composite section (as suggested by Hagelberg et al. [1992], table 1). A more complex procedure entails rescaling on a core-by-core basis; this method was adopted for high-resolution thermal conductivity measurements by the Shipboard Scientific Party (1996, equations 20–22). Another method, which is proposed for Leg 171B post-cruise application, is to rescale the spliced record to a downhole log (Harris et al., 1995).

During Leg 171B, it was not generally possible to develop complete composite sections, so we did not generate a formal mcd scale for each site. Intervals over which complete splicing was possible can be investigated using floating sections of a composite depth scale.

ORGANIC GEOCHEMISTRY

Shipboard organic geochemistry was used for research and to monitor the chance of encountering light hydrocarbons, H_2S, CO, CO_2, and other potentially hazardous gases during drilling opera-

Table 5. Normal polarity intervals for the Cenozoic and Cretaceous periods.

Normal polarity interval (Ma)		Polarity subchron
Top	Bottom	
0.000	0.780	C1n
0.990	1.070	C1r.1n
1.201	1.211	C1r.2n
1.770	1.950	C2n
2.140	2.150	C2r.1n
2.581	3.040	C2An.1n
3.110	3.220	C2An.2n
3.330	3.580	C2An.3n
4.180	4.290	C3n.1n
4.480	4.620	C3n.2n
4.800	4.890	C3n.3n
4.980	5.230	C3n.4n
5.894	6.137	C3An.1n
6.269	6.567	C3An.2n
6.935	7.091	C3Bn
7.135	7.170	C3Br.1n
7.341	7.375	C3Br.2n
7.432	7.562	C4n.1n
7.650	8.072	C4n.2n
8.225	8.257	C4r.1n
8.699	9.025	C4An
9.230	9.308	C4Ar.1n
9.580	9.642	C4Ar.2n
9.740	9.880	C5n.1n
9.920	10.949	C5n.2n
11.052	11.099	C5r.1n
11.476	11.531	C5r.2n
11.935	12.078	C5An.1n
12.184	12.401	C5An.2n
12.678	12.708	C5Ar.1n
12.775	12.819	C5Ar.2n
12.991	13.139	C5AAn
13.302	13.510	C5ABn
13.703	14.076	C5ACn
14.178	14.612	C5ADn
14.800	14.888	C5Bn.1n
15.034	15.155	C5Bn.2n
16.014	16.293	C5Cn.1n
16.327	16.488	C5Cn.2n
16.556	16.726	C5Cn.3n
17.277	17.615	C5Dn
18.281	18.781	C5En
19.048	20.131	C6n
20.518	20.725	C6An.1n
20.996	21.320	C6An.2n
21.768	21.859	C6AAn
22.151	22.248	C6AAr.1n
22.459	22.493	C6AAr.2n
22.588	22.750	C6Bn.1n
22.804	23.069	C6Bn.2n
23.353	23.535	C6Cn.1n
23.677	23.800	C6Cn.2n
23.999	24.118	C6Cn.3n
24.730	24.781	C7n.1n
24.835	25.183	C7n.2n
25.496	25.648	C7An
25.823	25.951	C8n.1n
25.992	26.554	C8n.2n
27.027	27.972	C9n
28.283	28.512	C10n.1n
28.578	28.745	C10n.2n
29.401	29.662	C11n.1n
29.765	30.098	C11n.2n
30.479	30.939	C12n
33.058	33.545	C13n
34.655	34.940	C15n
35.343	35.526	C16n.1n
35.685	36.341	C16n.2n
36.618	37.473	C17n.1n
37.604	37.848	C17n.2n
37.920	38.113	C17n.3n
38.426	39.552	C18n.1n
39.631	40.130	C18n.2n
41.257	41.521	C19n
42.536	43.789	C20n
46.264	47.906	C21n
49.037	49.714	C22n
50.778	50.946	C23n.1n
51.047	51.743	C23n.2n
52.364	52.663	C24n.1n
52.757	52.801	C24n.2n
52.903	53.347	C24n.3n
55.904	56.391	C25n
57.554	57.911	C26n
60.920	61.276	C27n
62.499	63.634	C28n
63.976	64.745	C29n
65.578	67.519	C30n
67.640	68.657	C31n
70.969	71.314	C32n.1n
71.643	73.635	C32n.2n
74.021	74.133	C32r.1n
74.470	79.650	C33n
83.500	120.396	C34n
121.000	123.673	M1n
124.051	124.721	M3n
126.723	127.669	M5n
128.176	128.313	M6n
128.425	128.580	M7n
128.966	129.276	M8n
129.508	129.774	M9n
130.221	130.556	M10n
130.874	131.201	M10Nn.1n
131.252	131.570	M10Nn.2n
131.588	131.880	M10Nn.3n
132.069	132.679	M11n
133.025	133.060	M11r.1n
133.350	133.627	M11An.1n
133.641	133.911	M11An.2n
133.988	134.216	M12n
134.777	134.846	M12r.1n
134.999	135.248	M12An
135.338	135.525	M13n
135.843	136.044	M14n
136.675	137.222	M15n
137.877	139.631	M16n
140.335	140.790	M17n
142.404	143.021	M18n
143.476	143.616	M19n.1n
143.703	144.691	M19n.2n

Notes: Cenozoic intervals are after Cande and Kent (1995). Cretaceous intervals are after Gradstein et al. (1995).

tions. The scheme for sampling and analyzing gas monitoring is based on the approaches developed during Leg 100, when the *JOIDES Resolution* was fitted with the chemistry laboratory (Emeis and Kvenvolden, 1986; Kvenvolden and McDonald, 1986). These approaches have been changed during subsequent legs, and also for Leg 171B, to fit the different requirements of the scientists as well as new shipboard instrumentation.

Prognosis for Gas Occurrence

Biogenic Methane

Biogenic methane is ubiquitous in thermally immature marine sediments and can occur either as free gas or gas hydrate. Methane gas hydrate above a zone of free methane in sediment pores is common north of the Leg 171B transect (Kvenvolden and McMenamin, 1980; Holbrook et al., 1996; Paull, Matsumoto, Wallace, et al., 1996). Methane gas hydrates break down rapidly at sea-surface conditions and release methane. Recent seismic studies show that in the nearby Blake-Bahama Outer Ridge area, methane gas hydrate is common from about 200 to 450 mbsf, and free methane occurs at depths of at least 250 m below this level (Holbrook et al., 1996). A bottom simulation reflector (BSR) is a primary indicator for gas hydrates at depth in the Blake-Bahama Outer Ridge area. Some holes drilled during Leg 171B were scheduled to reach total depth at 600–700 mbsf and were expected to contain biogenic methane. Because a BSR does not occur along the Leg 171B drilling transect (United States Geological Survey multichannel seismic [USGS MCS] Line TD-5; see Fig. 3 in the "Introduction" chapter, back-pocket foldout, this volume), it was assumed that small quantities of methane would be encountered during the Leg 171B transect.

The chance that gaseous hydrocarbons have been generated in the sediments to be drilled during Leg 171B can be inferred from organic geochemistry studies on samples collected during Deep Sea Drilling Project (DSDP) Leg 44 at Sites 390, 391, and 392 (Benson et al., 1978; Tissot et al., 1979; Katz, 1983b). Site 390 was redrilled at Site 1049 on the eastern end of the Leg 171B depth transect. Site 391 is in the Blake-Bahama Basin to the southeast of Site 1049, and Site 392 is on the Blake Nose, 22 km south of Site 390. Organic geochemistry

results from Sites 390 through 392 indicate that the sediments we planned to drill during Leg 171B may contain low to moderate amounts of kerogen (about 0.2 to 2 wt% total organic carbon [TOC]) that is generally lean in hydrogen content and dominantly of humic origin.

From east to west across the Leg 171B transect, an increasing amount of kerogen in the core is possible because of increased accumulation rates of gas-prone humic debris from the North American continent. This debris is composed of lean source rocks for type III kerogen and does not have the potential to produce large quantities of gas.

Extrapolation of vitrinite reflectance data collected by Cardoso et al. (1978) and Dow (1978) to the Leg 171B transect suggests that the oil window occurs at about 2000 mbsf. Because the Leg 171B sites were scheduled to reach only about 600 mbsf and the vertical permeability of the strata below the sites is considered low, the probability of encountering in situ or migrated thermogenic gas was considered low.

Potential Gas Traps

Leg 171B traversed a simple east-dipping homoclinal structure that in seismic section appears to have no significant structural traps (USGS MCS Line TD-5; see Fig. 3 in the "Introduction" chapter, back-pocket foldout, this volume). Stratigraphic pinch-outs that may form traps are seen in the seismic section to the west of Site 1052. However, penetration of the apex of these traps along the transect was not planned; therefore, no gas or oil accumulations were expected.

Gas Analyses

Real-time gas monitoring required taking one headspace gas sample per core in the initial hole drilled at each site. Additional headspace gas samples were taken from any voids or gas pockets in the recovered cores. The A hole at each site on this leg was routinely monitored for gases, and when hazardous gases were detected in the a hole, all subsequent holes were monitored at that site.

The techniques for extracting the disseminated gas into a headspace gas sample and for gas analysis mostly follow those described for Leg 139 (Shipboard Scientific Party, 1992).

Gas Composition

In the headspace method, gases released from the sediments after core recovery were analyzed by gas chromatography. Immediately after arriving on deck, a cork borer of about 1 cm in diameter was used to obtain a small volume of sediment midway along the core. This sediment sample of about 5 cm^3 was placed in a 21.5-cm^3 glass serum vial, which was sealed with a Teflon septum and a metal crimp cap. When consolidated or lithified sediments were recovered, chips of the cored material were placed in the glass vial and were sealed. The vial was then heated for 30 min in an oven at a constant temperature of 60°C. A 5-cm^3 volume of the gas from the headspace of the vial was extracted with a gas-tight glass syringe for direct injection into the gas chromatograph column.

Gas pockets in sediment or rock were sampled using pre-evacuated, 20-cm^3 glass tubes fitted with rubber septums (vacutainers). The vacutainers were attached to a tool with a valve and a needle, which was used to puncture the core liner.

Using a gas-tight, glass syringe, all headspace gas and vacutainer samples were injected into one of the following gas chromatographs, depending on gas concentration. For low gas concentrations, a Hewlett-Packard model 5890 II Plus gas chromatograph, equipped with a flame ionization detector (FID) and a 2.4 m × 0.32 cm stainless-steel column packed with HayeSep S (100–120 mesh), was used. Concentrations of methane, ethane, and propane were routinely obtained with this gas chromatograph.

If higher concentrations of ethane and heavier hydrocarbons (C_{2+}) were suspected, gas samples were analyzed using the natural gas analyzer (NGA). The NGA consists of a Hewlett-Packard model 5890 II Plus gas chromatograph fitted with an FID and thermal conductivity detector (TCD). The triple-column plumbing and operating conditions were identical to those described for Leg 139 (Shipboard Scientific Party, 1992), except that a new type of column for the FID was installed for Leg 171B. A HP-PLOT (porous layer open tubular) Al_2O_3 column with a 15 m × 0.53 mm × 15 µm film thickness capillary tube was used, giving enhanced hydrocarbon resolution. All gas chromatograph operation controls, data acquisition, and data processing were conducted using the Hewlett-Packard Chem Station. Alkane hydrocarbons from methane to hexane, as well as CO_2, CO, CS_2, H_2S, N, and O, if found in quantity, were routinely monitored with the NGA. All gas concentrations are reported in parts per million (ppm [volume/volume]).

The gas analyzers monitor two hazards: (1) the development of flammable or explosive conditions and (2) the possibility of a hydrocarbon seep or blowout occurring in a hole. Because biogenic gas is ubiquitous in marine sediments, its presence is expected in minor amounts, and its detection alone is not necessarily indicative of hazardous conditions. Thermogenic gases are detected using longer chain (C_{2+}) alkanes. That thermogenic gases can occur in large quantities in shallow marine sediments greatly increases the chances for hazardous drilling conditions.

The volume ratio of methane to ethane (C_1/C_2), calculated from gas analyses, is useful in identifying the source of hydrocarbon gases. C_1/C_2 values on the order of 1000 are typical for immature marine sediments. C_1/C_2 values approaching 100 and C_1 reaching 30% to 50% of total gas suggest that some thermogenic gas is present and indicate that hazardous conditions could exist.

Shipboard laboratory air was found to contain about 2 ppm methane. This value is the practical detection limit for methane using the shipboard headspace method.

Elemental Analyses

One 2-cm^3 sediment sample was routinely taken from each core for analysis of total carbon (TC), total inorganic carbon (TIC), TOC, total hydrogen (TH), total sulfur (TS), and total nitrogen (TN). Samples of 20 cm^3 of moderate- to dark-colored sediment were also taken to determine their elemental composition; other analyses were performed if indicated. Samples with TOC >0.5 wt% were submitted for Rock-Eval pyrolosis and organic petrography. The procedures for elemental analysis were similar to those used during Leg 139 (Shipboard Scientific Party, 1992).

TIC concentrations were measured using a Coulometrics 5011 carbonate-carbon analyzer. An aliquot of ~10 mg of freeze-dried, finely ground sample was reacted with excess 2N HCl in the coulometer sample tube. The liberated CO_2 was scrubbed first by a 45 wt% aqueous KOH solution and then by a saturated $AgNO_3$ solution to remove the acidic gases and sulfur compounds that can interfere with the titration. The scrubbed CO_2 was quantitatively dissolved in the Coulometer cell solution to form a titratable acid that causes the blue color of an indicator solution to fade. Titration of the acid occurs when a base electrically generated in the Coulometrics cell neutralizes the dissolved CO_2, causing the indicator color to return toward the original blue end-point. The indicator color change was monitored by a photodetector cell. At the end-point, the total amount of base equivalent required to neutralize the acid was used to compute the amount of inorganic carbon in the sample, which is reported as weight percent TIC. The percentage of carbonate was calculated from the TIC content assuming that all inorganic carbon was present as pure calcium carbonate (calcite):

$$CaCO_3 = TIC \times 8.33.$$

The presence of dolomite and siderite bias the determination of TIC because they do not completely dissolve in the time allowed for digestion. Therefore, coulometric carbonate-carbon measurements provide minimum estimates of inorganic carbon content.

Total carbon, hydrogen, nitrogen, and sulfur (CHNS) were determined with a Carlo Erba 1500 CNS analyzer, using helium as a carrier gas. For CHNS analysis, about 5–20 mg of freeze-dried, ground sediment was combusted at a temperature of 1000°C in a stream of high-purity oxygen. The darker the sediment, the lower the sample mass required for analysis. After combustion, excess oxygen was removed, and the gaseous combustion products were chemically reduced. The reduced gases were separated by gas chromatography and quantified with a TCD. TOC contents were calculated as the difference between TC and TIC:

$$TOC = TC - TIC.$$

The precision ($\pm 1\sigma$ standard deviation) of these analyses was typically between ±2% and ±3% of the measured value. Negative values of TOC that were computed by this method are reported as zero. TOC, TH, TS, TN, TIC, and TC are reported as weight percent.

During the analysis of some high-TOC samples from Hole 1049B, the TOC from Rock-Eval analysis was found to be about 10% lower than TOC computed from coulometric analysis. This difference is attributed to the low-TOC standards used to calibrate the Rock-Eval system.

Organic Matter Type, Richness, and Maturity

A Delsi-Nermag Rock-Eval II system was used to monitor disseminated organic matter type, richness (concentration), maturity, and oil shows during drilling operations. Using regression methods, Rock-Eval data collected as a function of depth can be extrapolated to indicate the depth where thermally mature rock and thermogenic hydrocarbons can be expected. In addition, when examined along a depth profile in a hole, abrupt local changes in the Rock-Eval S_1 peak can be an indication of oil shows or bitumen staining that may signal dangerous conditions in what other data suggest are immature sediments.

Rock-Eval Pyrolysis

Rock-Eval pyrolysis is a whole-rock assay technique that entails heating small quantities of rock and measuring the mass of hydrocarbon gases evolved as a function of temperature (Tissot and Welte, 1984; Espitalié et al., 1986). Detailed definitions for the Rock-Eval analytical reports are given in Table 6. Samples with ≥0.5 wt% TOC were freeze-dried and pulverized. The aliquot mass was usually about 100 mg. The Rock-Eval system heats the powdered rock through a temperature program under anhydrous conditions. The first stage in the temperature program was to hold the sample at 300°C for 3 min, which caused the sorbed and free hydrocarbons in the sample to be driven off and recorded as the S_1 peak. The second stage of the temperature program was to increase temperature from 300° to 550°C at 25°C/min. Second-stage heating caused organic matter in the sample to crack and form several compounds. The hydrocarbons and CO_2 formed were recorded as the S_2 and S_3 peaks, respectively, and other compounds formed were not analyzed. S_1 and S_2 hydrocarbons were measured by an FID and are reported as milligrams of hydrocarbons (HC) per gram of rock. Between 300° and 390°C of the second-stage temperature program, CO_2 released from the thermal cracking of organic matter (S_3) was trapped and later measured by a TCD and reported as milligrams of CO_2 per gram of rock. CO_2 generated during this step was measured during cooling after the second-stage temperature program was completed and acquisition of the S_4 peak was complete.

In the Rock-Eval II plus TOC analyzer, after the S_2 peak was recorded, the remaining carbon was oxidized by introducing oxygen to the sample while it was at 600°C. The CO_2 obtained from the subsequent oxidation was recorded as the pyrolyzable carbon, or S_4 peak, and was reported as milligrams of CO_2 per gram of rock. TOC was computed from the sum of the S_1, S_2, and S_4 peaks and reported as weight percent TOC. S_3 was not included because it was considered negligibly small, and the oxygen-bearing carbon in kerogen is not important for assessing hydrocarbon potential (Bordenave et al., 1993).

The analytical results of Rock-Eval pyrolysis are unreliable if the TOC content of the rock sample is <0.5 wt% (Peters, 1986; Bordenave et al., 1993). Samples with <0.5 wt% TOC are included in the data tables but are not included in the interpretative plots.

It must be emphasized that Rock-Eval pyrolysis gives only a semiquantitative estimate of organic matter properties because rapid heating to extreme temperatures under dry conditions does not appropriately mimic natural thermal maturation in basins. Rock-Eval results are best interpreted using the broad trends of grouped data and ignoring outlier data. Even within these limitations, comparing the trends obtained by Rock-Eval analysis against other analyses, such as thermal maturation and elemental analyses, shows that it is a useful indicator of thermal maturation and petroleum generation potential (Katz, 1983a; Peters, 1986; Langford and Blanc-Valleron, 1990; Bordenave et al., 1993). The general consensus is that Rock-Eval pyrolysis data, along with vitrinite reflectance and kerogen petrography, can be used to qualitatively evaluate the source rock's tendency for oil and gas generation, past and residual hydrocarbon generation capacity, and thermal maturity (Tables 7, 8).

Besides the technical limitations of Rock-Eval analysis, organic matter contaminants and naturally occurring oils and bitumens can interfere by increasing the S_1 and S_2 values. Hydrocarbon migration is detected as local occurrences of samples with an S_1 peak >2 mg HC/g rock, an anomalously high transformation ratio (TR), and low maximum temperature (T_{max}; Table 6) compared with adjacent samples, and a bimodal S_2 peak. As a consequence, hydrocarbon migration makes the transformation ratio an ambiguous indicator of thermal maturation. Generally, no oil-staining or immature bitumen was observed in the samples collected during Leg 44 drilling in the vicinity of Leg 171B; consequently, hydrocarbon migration was not expected to be an important factor in Rock-Eval analysis.

Fluorescence Microscopy and Vitrinite Reflectance

A portion of the whole rock or freeze-dried sediment remaining after elemental analysis was prepared for fluorescence microscopy and vitrinite reflectance analysis by splitting it into two samples. A kerogen concentrate was prepared from one split by digesting about 10 g of large sediment pieces in dilute 10% HCl. The kerogen concentrate was prepared as a smear mount by embedding it in cold-setting, ultraviolet-activated Norland type 61 optical adhesive on a glass slide without a cover slip. The slide was hardened by a 10-min exposure to ultraviolet light in a Btek model BUV-3B Eprom eraser. The smear slide was used without polishing to determine kerogen type and the thermal alteration index (TAI). The slide was then polished and used to determine vitrinite reflectance. If the smear mount of kerogen had a sufficient amount of humic debris, a portion of the remaining sample split was used to make whole-rock mounts by coarsely crushing and screening the sample to a size between 1.7 and 0.25 mm to allow reflectance measurements on randomly oriented vitrinite embedded in the larger host-rock pieces. The crushed and screened whole-rock samples were embedded in cold-setting plastic resin (Epotek 301) and were vacuum impregnated. The smear-slide and screened-sample mounts were polished using the procedure of Pawlewicz (1986). Embedding and polishing crushed and screened samples produces many randomly oriented pieces of kerogen that are still contained within the host-rock pieces. This method produces random reflectance measurements that are comparable to the results

Table 6. Rock-Eval analytical values and derived parameters.

Reported value	Reported as	Indication	Interference
S_1 is the first peak of HC yield occurring during pyrolysis.	mg HC/g rock or sediment	Sorbed or free HC from kerogen or the host rock or sediment	HC migration, organic or HC contamination of sample
S_2 is the second peak of HC yield released by thermal cracking of kerogen.	mg HC/g rock	HC generation potential remaining in the kerogen	HC migration, organic or HC contamination of sample
S_3 is the CO_2 released from the thermal cracking of kerogen.	mg CO_2/g rock	Oxygen content of kerogen	Organic contamination of sample
S_4 or pyrolysible carbon	mg CO_2/g rock	Pyrolysible organic carbon content remaining after acquisition of the S_2 peak	HC migration, organic or HC contamination of sample
TOC = $S_1 + S_2 + S_4$	wt% TOC	Organic carbon content of kerogen	HC migration, organic or HC contamination of sample; high S_3 such as coal samples will have lowered TOC.
T_{max} is the temperature at which the maximum kerogen breakdown occurs within the S_2 peak.	Degrees Celsius	Thermal maturation of sample	Low T_{max} may be related to broad S_2 peaks caused by low TOC values or migrated bitumen in the sample.
HC index = S_2/S_3	mg HCmg CO_2	Kerogen type	HC migration
TR or PI = $S_1/(S_1 + S_2)$	Dimensionless	Extent of hydrocarbon generation but may be influenced by migrated HC	HC migration, locally high TR indicates oil show or bitumen staining
HI = $(S_2/TOC) \times 100$	mg HC/g TOC	H content of the kerogen	HC migration
OI = $(S_3/TOC) \times 100$	mg CO_2/g TOC	O content of the kerogen	Organic contamination of sample
Genetic potential = $S_1 + S_2$	mg HC/g rock	Total HC generation capacity	HC migration

Notes: HC = hydrocarbon; TOC = total organic carbon; TR = transformation ratio; PI = production index; HI = hydrogen index; OI = oxygen index.

Table 7. Source rock potential vs. TOC, thermal maturity, and hydrogen content of kerogen.

Richness	Genetic potential	Generated petroleum type		Thermal maturity		Source rock potential
TOC wt%	S_1+S_2 (mg HC/g rock)	HI (mg HC/g C)	H/C index; S_2/S_3 (mg HC/g CO_2)	T_{max} (°C)	Vitrinite reflectance (mean random in %)	Interpreted from kerogen analysis
<0.5	Mudrock: <0.5 poor limestone: <0.5 poor to fair (?)	Usually unreliable	Usually unreliable	Usually unreliable	Maybe unreliable	Probably not a source rock
0.5 to 2	<5 poor 10 good >15 excellent	< 200 gas; 200-300 mixed (oil and gas); >300 oil	Unreliable	< 425 immature; 425-470 mature >470 post mature	< 0.5 immature; 0.5-1.3 mature >1.3 post mature	Marginal source rock: probably not capable of expelling oil
0.5 to 2	<5 poor 10 good >15 excellent	< 200 gas; 200-300 mixed; >300 oil	<2.5 dry gas; 2.5-5 wet gas; >5 oil	--or-- >425 oil; >470 wet gas then dry gas	--or-- >0.5 oil; >1.3 wet gas then dry gas	May not be an effective source rock as it may not expel oil
>2 to 5 fair/good; >5 good; >10 excellent	<5 poor 10 good >15 excellent	< 200 gas; 200-300 mixed; >300 oil	<2.5 dry gas; 2.5-5 wet gas; >5 oil			Fair grading to excellent source rock as HI and TOC increase

Note: Compiled from Peters (1986), Robert (1988), Langford and Blanc-Valleron (1990), and Bordenave et al. (1993).

of the reflectance analyses on kerogen concentrates, while preserving the original rock structure around the kerogen grains. This is a key element in detecting first-cycle vitrinite (Tables 9, 10). Reflected white light and fluorescence microscopy were used during the cruise to identify organic matter type and to assess its TAI. Comparison with Rock-Eval analysis used the correlation listed in Table 8. The vitrinite reflectance of these polished samples was measured after the Leg 171B cruise. Type I vitrinite was used for the analysis of reflectance (Table 11).

In kerogen, vitrinite selection for analysis can be difficult because several different populations of vitrinite, or vitrinite-like material, can exist in one sample. During Leg 171B, vitrinite was characterized under reflected white light and fluorescence excitation by the classification given in Table 11. The description and identification of other materials in kerogen uses the nomenclature given in Stach et al. (1982) and Robert (1988).

INORGANIC GEOCHEMISTRY

Interstitial-Water Sampling and Chemistry

The interstitial-water program used 5- to 15-cm-long whole-round sediment sections, which were cut and capped immediately after the cores arrived on deck. For one hole at each site, one whole-round sample was taken from each of the first six cores and from every third core thereafter to total depth. Before squeezing, the samples were removed from the core liner and the outside surfaces were carefully scraped off with spatulas to minimize potential contamination. The whole-round samples were placed in a titanium and stainless-steel squeezing device and were squeezed at ambient temperature with a hydraulic press. The interstitial-water samples were collected in plastic syringes, filtered through 0.45-µm disposable filters, and then either stored in plastic sample bottles for shipboard analyses or archived in glass ampoules and/or heat-sealed plastic tubes for shore-based analyses.

Interstitial-water analyses followed the procedures outlined by Gieskes et al. (1991). Interstitial-water samples were analyzed for salinity with a hand-held refractometer and for pH and alkalinity by Gran titration with a Brinkman pH electrode and Metrohm autotitrator. Na^+, K^+, Ca^{2+}, Mg^{2+}, and SO_4^{2-} concentrations were analyzed routinely by ion chromatography using a Dionex DX-100 ion chromatograph. Cl^-, Ca^{2+}, and Mg^{2+} concentrations were measured routinely by titration. H_4SiO_4, NH_4^+, and B concentrations were measured by color spectrophotometric methods with a Milton Roy Spectronic 301 spectrophotometer. Li^+, Sr^{2+}, and Rb^{2+} concentrations were measured by flame spectrophotometric techniques with a Varian SpectrAA-20

Table 8. Correlation of rank parameters relative to the rank of humic kerogen or coal.

Approximate hydrocarbon generation stages for oil generative organic matter	Coal rank (U.S.A.)	Rv-r (%)	Rock-Eval T_{max} (°C)	TR	CAI	TAI	C (%)	VM (%)	H_2O (%)	Peak burial temp. (°C)
Biogenic gas	Peat	0.2	410			1	60	70		6
	Lignite	0.3	415		1		60	60	75	39
	Sub-bituminous	0.4	420		1	2	71	52	35	62
Near end for biogenic gas	High vol. bit. C	0.5	427		1.5		73	46	25	80
Near onset of thermogenic oil		0.6	435	0.10	2	2.5	77	44		95
Near onset thermogenic gas-coal	High vol. bit. B	0.7	440		2		77	40	8	107
	High vol. bit. A	0.8	445	0.20	2-3	3		37		118
	High vol. bit. A	0.9	452	0.40	2-3			35		128
Near peak oil generation	High vol. bit. A	1.0	460	0.60	2-3			33		136
Onset gas generation: type I and II	Medium vol. bit.	1.1	465	0.70	3	3.5				144
		1.2	472		3		87	28		151
Near onset oil cracking		1.3	480	0.85	3		87	28		157
		1.4	485		3					163
	Low vol. bit.	1.5	490	0.90	3	4		22		169
		1.6	498		3			19		174
Limit of oil preservation		1.7	503	0.98	3					179
		1.8	510		3					184
	Semi-anthracite	1.9	515		3-4			14		188
Near onset of dry gas		2.0	520		3-4					192
		2.1	528		3-4			12		196
		2.2	535		4					200
		2.3	540		4			10		204
		2.4			4					207
		2.5			4	5				210
		2.6			4		91	8		213
	Anthracite	2.7			4					217
		2.8			4					219
		2.9			4			6		222
		3.0			4					225
		3.1			4			5		228
		3.2			4			5		230
		3.3			4			5		233
		3.4			4					235
Near onset of economical gas		3.5			4		93.5	4		238

Notes: Rv-r = mean random vitrinite reflectance; Rock-Eval = Rock-Eval pyrolysis; TR = transformation ratio; CAI = conodont alteration index; TAI = thermal alteration index; VM = volatile matter; temp. = temperature; vol. = volatile; bit. = bituminous. Compiled from Stach et al. (1982), Bustin et al. (1983), Tissot et al. (1987), Robert (1988), and Barker and Pawlewicz (1993).

Table 9. Recognition of first-cycle vitrinite in whole-rock mounts.

Appearance of vitrinite grains
1. Vitrinite grain length/width »1. Woody DOM tends to be elongate.
2. Wispy form of vitrinite grain. Woody DOM is deposited as a pliable, frayed, or shredded-looking grain.
3. May show framework grain impressions. Caused by compaction of pliable, first-cycle grains.
4. Uniform polish hardness in unweathered samples. Variation of polish hardness suggests weathering and may indicate a recycled grain.
5. No zoned reflectance in unweathered samples. Reflectance zones or rims of lower reflectance suggest a weathered grain; in an unweathered sample, zoned reflectance suggests it is recycled.
6. No abrasion rounding. If rounded, grains are interpreted to be caused by transport, indicating recycled DOM. Caution needs to be used when employing this criteria as some DOM grains, such as vesinite or corpocollinite bodies, are rounded when formed.
7. No external brittle fracture surfaces on isolated pieces. A brittle fracture of the grain observed as an abrupt truncation of grain structure may suggest the grain has been previously gelified and that, during recycling, portions of it have been broken off.
8. Grains consisting of trimacerites showing a layered texture or desmocollinite. These maceral associations indicate the grain has been recycled.

Note: DOM = dispersed organic matter.

Table 10. Distinguishing vitrinite from solid bitumen.

Vitrinite
1. Always a framework grain.
2. First-cycle vitrinite conforms to bedding and may interdigitate with enclosing matrix or drape framework grains (i.e., the grain is initially not rigid.)
3. May show primary maceral associations, such as resinite filling cell lumens, and so forth.
4. Cell lumens may be observed.
5. Only observed in depositional sedimentary features, not diagenetic features.
6. May show compaction features (pinch texture, wrapping around or conforming to the shape of framework grains, and so forth).
Solid bitumen
1. Typically observed as a product of diagenesis and in diagenetic features (fractures, cements, secondary porosity).
2. Typically shows no primary, depositional association with other macerals.
3. Tends to be internally homogeneous.
4. Typically shows textures consistent with being deposited or precipitated on framework grains, on cement, or in pore space.
5. May impregnate rock matrix.
6. Typically originates during diagenesi; consequently, compaction textures are reduced in magnitude, or absent, compared with primary DOM.

Note: DOM = dispersed organic matter.

atomic absorption spectrometer. The International Association of Physical Sciences of the Ocean (IAPSO) standard seawater was used for calibrating techniques, when applicable. The reproducibility of these techniques, expressed as 1σ standard deviations of means of multiple determinations of IAPSO standard seawater or of a standard treated as a sample, are alkalinity, 2%; Cl^-, 0.4%; Ca^{2+}, <1%; Mg^{2+}, 0.5%; SO_4^{2-}, 2%–3%; H_4SiO_4 and B, 1%–3%; NH_4^+, 2%–5%; Li^+ and Sr^{2+}, 2%–4%; Na^+, 5%; and K^+, 4%. Sodium was also determined with better precision (~0.4%) by charge balance, neglecting contributions by ammonium, and these are the values reported. Chemical data for interstitial-water analyses are reported in molar concentration units in each site chapter.

PHYSICAL PROPERTIES

Shipboard measurements of physical properties provide information that assists in the characterization of lithologic units, the correlation of lithology with downhole geophysical logging data, the nature of consolidation, and the interpretation of seismic reflection profiles.

Table 11. Kinds of vitrinite observed in whole-rock mounts.

Type	Kind of vitrinite	Description
I	First-cycle vitrinite	In SOM, this is the vitrinite group material that has the best qualities for thermal maturity assessment purposes. It has an elongate to very elongate shape, lies on apparent bedding surfaces, and can show wispy form and/or interfingering with the enclosing sediment. May also show pinch textures or other compaction effects resulting from the burial of what is initially a soft deformable grain. At least a portion of the surface is unflawed and large enough to allow measurement, or the grain is classed as a vitrinite III.
II	Fluorescent vitrinite	Vitrinite that shows fluorescence under blue-light excitation. A characteristic of vitrinite that shows suppressed reflectance; that is, lower than vitrinite I reflectance. Vitrinite II reflectance must be corrected to related vitrinite I levels.
III	Flawed vitrinite	Like vitrinite I, but it has a pitted or otherwise poorly polished surface. The reflection of this material is usually less than that of vitrinite I. As the polished surface improves, vitrinite III reflectance can approach that of vitrinite I. In dispersed organic matter (DOM) samples, its shape is subelongate to equant (blocky). May show breakage surfaces/truncation of elongation.
IV	Recycled vitrinite	Redeposited vitrinite. These grains may show zoned or mottled reflectance and/or rounding because of alteration and sedimentary transport after initial coalification. The grains may also show weathering effects such as low reflecting rims at grain edge, variable polish hardness, and microfissures. May also occur as a plied bimacerite and trimacerite grains formed by recycled coal.
V	Altered vitrinite	Vitrinite that has the form of vitrinite I but a higher reflectance. Apparently altered by degradation or oxidation. Like semifusinite of coal macerals, grades from inertinite to near vitrinite-I reflectance levels.

Notes: DOM = dispersed organic matter; SOM = sedimentary organic matter (DOM and coal). Vitrinite I and II from Gutjahr (1983). Samples from drill cuttings may also contain vitrinite derived from uphole cavings.

The objectives of the physical properties program of Leg 171B, in addition to providing a link between the lithologic and geophysical data, includes the collection of high-resolution data for construction of composite stratigraphic sections.

Several types of measurements were performed on whole-round sections. Nondestructive measurements of bulk density, magnetic susceptibility, transverse compressional-wave velocity, and natural gamma radiation were made using the MST. The MST incorporates the GRAPE, magnetic susceptibility meter (MSM), compressional-wave (*P*-wave) logger (PWL), and natural gamma-ray (NGR) radiation sensor. Thermal conductivity was measured at discrete intervals in whole-round sections using the needle probe method.

Physical properties measurements made on split-core sections included undrained shear strength, longitudinal and transverse compressional-wave velocity, and longitudinal and transverse resistivity. Index properties determined for discrete samples included wet bulk density, dry bulk density, grain density, water content, porosity, and void ratio.

To accommodate the generation of high-resolution MST data for hole-to-hole and intersite stratigraphic correlation, as well as the general shipboard physical properties objectives, a specific sampling strategy was formulated for Leg 171B. The generation of high-quality MST data was considered of paramount importance to meet the primary scientific objectives of this leg.

All physical properties measurements were routinely determined in the A hole at each site. Bulk density, magnetic susceptibility, and compressional-wave velocity, measured using the MST, were the only measurements routinely determined for the B and C holes. Compressional-wave velocity was measured with the MST only for cores recovered with the APC because XCB and RCB cores typically have a poor core liner/sediment contact.

Whole-round sections were first passed through the MST. The MST sampling frequency was dependent upon the sediment lithology and the time available. Thermal conductivity was then measured on alternate whole-core sections. After the sections were split, compressional-wave velocity, undrained shear strength, and resistivity were determined at a frequency of one measurement per alternate split-core section. Discrete samples were then selected for the measurement of index properties at a frequency of one per section or alternate sections. Wherever possible, all physical properties measurements were determined for the same section interval to allow correlation of the data sets.

MST Measurements

GRAPE measurements of bulk density are determined by comparing the attenuation of gamma rays through the core material with attenuation through aluminum/seawater standards (Boyce, 1976; Shipboard Scientific Party, 1997). Bulk density data are of higher quality when determined on APC cores because the liner is generally completely filled with sediment. In XCB and RCB cores, GRAPE measurements cannot be used to reliably determine bulk density.

The measurement width of the GRAPE sensor is ~5 mm, and this was taken into account in choosing a sampling frequency. The minimum integration time for a statistically significant GRAPE measurement is 2 s, and during Leg 171B, routine GRAPE measurements used a 4-s integration time. A freshwater control was run with each section to measure instrument drift.

Magnetic susceptibility was measured with the MST using a Bartington MS2 meter with an 8-cm-diameter loop. The measurement width of the MSM sensor is ~4 cm, with a minimum statistically significant count time of 1–4 s, depending on lithology. During Leg 171B, magnetic susceptibility was routinely measured at a spacing and precision dictated by the susceptibility of the sediment and the time available. The principal aim during data acquisition was to achieve at least a 5-cm resolution where the sediment magnetic susceptibility was high enough to achieve this within a reasonable time frame. The quality of susceptibility data degrades in XCB cores where the core liner may be incompletely filled, although the data can still be used for stratigraphic correlation. The magnetic susceptibility data were not corrected for incomplete sediment volume.

Transverse *P*-wave velocity was measured on the MST track using the PWL for all APC cores. The measurement width of the PWL is ~1 mm. In addition to velocity, signal strength, which allows the operator to distinguish anomalous values caused by poor transducer/liner or core liner/sediment contact, was also collected. Calibration was performed using a core liner filled with distilled water. The PWL was not used on XCB or RCB cores because the core liner/sediment interface is usually poor.

Natural gamma radiation was measured using the NGR on the MST. The measurement width of the NGR is ~15 cm, with a statistically significant count time of at least 15 s, depending on lithology. Following the current data collection routine, data from 256 energy channels were collected and archived. For presentation purposes, the counts were summed over the range of 200–3000 keV to be comparable with data collected on previous legs. This integration range also allows direct comparison to be made with downhole logging data, which are collected over a similar integration range. No corrections were made to NGR data from the XCB or RCB cores to account for sediment incompletely filling the core liner.

Index Properties

Index properties (wet and dry bulk density, grain density, water content, porosity, and void ratio) were determined from measurements of wet- and dry-sediment mass and dry-sediment volume. Dis-

crete samples of ~10 cm^3 were taken from soft sediments with a plastic sampling tube and were placed in 10-mL beakers. In firm sediment, minicores were cut using a $^7/_8$-in ID coring bit.

Sample mass was determined to a precision of ±0.01 g using a Scientech 202 electronic balance. The sample mass was counterbalanced by a known mass such that only mass differences of <5 g were measured. The Scientech electronic balance was calibrated at sea using a five-point linear calibration, which included the following combinations of weights on the reference and sample balances, respectively: 0 g:0 g, 5 g:0 g, 10 g:5 g, 20 g:10 g, and 30 g:20 g. These calibration results compare favorably with those determined during Leg 170.

Whole-Pyrex-beaker density was determined by measuring the mass of selected beakers using the Scientech balance, and volume was determined using a Quantachrome Penta-Pycnometer. The mean density and standard deviation for five beakers was 2.22 g/cm^3 ± 0.01 g/cm^3, which is identical to the crushed-beaker density obtained during Leg 170 (K. MacKillop, pers. comm., 1997). The ODP physical properties moisture and density (MAD) database was updated with beaker volumes determined using the Leg 171B density value.

Sample volume was determined using the Quantachrome Penta-Pycnometer, a helium-displacement pycnometer. The Quantachrome pycnometer measures volume to an approximate precision of ±0.01 cm^3. Volume measurements were repeated as many as five times until three consecutive measurements yielded volumes with a relative precision of <0.01 cm^3. A reference volume was included within each sample set and was rotated sequentially among the cells for drift monitoring.

Individual index properties were calculated using measurements of wet- and dry-sediment mass and dry-sediment volume. This method is preferred over others because volume measurements of wet samples are less accurate than dry-volume measurements. The samples were oven dried at 105°C after the measurement of wet mass. Using MAD notation, the three measured values are

M_t = wet mass;
M_d = dry mass (mass of solids including mass of residual salt); and
V_d = dry volume (volume of solids including volume of residual salt).

Pore-water mass (M_{pw}), mass of solids (M_s), and pore-water volume (V_{pw}) can then be calculated:

$$M_{pw} = (M_t - M_d)/(1 - s),$$

$$M_s = M_t - M_{pw}\text{, and}$$

$$M_s = M_t - M_{pw}V_{pw} = M_{pw}/D_{pw},$$

where s and D_{pw} are pore-water salinity and density, respectively. The variations in pore-water salinity and density typically found in marine sediments do not affect the calculations significantly, and standard seawater values at laboratory conditions are used within the MAD calculation program:

s = 0.035
D_{pw} = 1.024 g/cm^3.

Wet volume (V_t) and volume of solids (V_s) are calculated as follows:

$$V_t = V_s + V_{pw}\text{ and}$$

$$V_s = V_d - V_{salt},$$

where

$$V_{salt} = [M_{pw} - (M_t - M_d)]/D_{salt}\text{ and}$$

D_{salt} = 2.257 g/cm^3.

Water content, expressed as a percentage, is calculated in terms of total mass of solids (W_s) and total mass (W_t):

$$W_s = (M_t - M_s)100/M_s\text{ and}$$

$$W_t = (M_t - M_s)100/M_t.$$

Bulk density (*BD*), grain density (*GD*), dry density (*DD*), porosity (*P*), and void ratio (*VR*) are calculated as follows:

$$BD = M_t/V_t,$$

$$GD = M_s/(V_t - V_{pw}),$$

$$DD = M_s/V_t,$$

$$P = (V_{pw}/V_t)100\text{, and}$$

$$VR = V_{pw}/(V_t - V_{pw}).$$

Thermal Conductivity

The thermal conductivity of cored material was measured in whole-core sections using the needle probe method in full-space configuration for soft sediments (von Herzen and Maxwell, 1959). Measurements were taken using either a five-probe Thermcon-85 unit or a single-probe TeKa (Berlin) TK-04 unit after all cores had equilibrated in their liners to laboratory temperature over ~4 hr. When the Thermcon-85 unit was used, all sections selected from a particular core were measured simultaneously, whereas individual sections were measured with the TK-04 when they became thermally equilibrated. Needle probes were inserted through small holes drilled in the core liner. To avoid contamination of the core material, thermal joint compound was not used. Thermal conductivity values were measured until the sediments became too indurated to insert the needle probes. Needle probes were sequentially circulated through a red rubber standard to measure drift (Thermcon-85) or were periodically checked against laboratory standards (TK-04).

Core sediment temperature was monitored by the thermistors in the needle probes, and the data acquisition sequence was initiated when the background temperature drift dropped below 0.04°C/min. To determine thermal conductivity, the core is heated while temperature is measured. The increase of temperature in the core should vary logarithmically with time such that

$$T(t) = (q/4\pi k)\cdot\ln(t) + L(t),$$

where k = thermal conductivity, T = measured temperature, t is the amount of time the heater is on, and q is the amount of heat input per unit length of probe per unit time. The term $L(t)$ quantifies the linear change in temperature with time and includes the background temperature drift and any linearity that results from instrumental errors and the geometrical inadequacies of the experiment. Data are reported in W/(m·K) and have an estimated error of 5%–10%.

Individual needle probes for the Thermcon-85 were calibrated to account for differences between true and measured thermal conductivity values by conducting a calibration experiment with four standards of known thermal conductivity. The black rubber, gelatin, red

rubber, and Macor ceramic standards have known thermal conductivities of 0.54, 0.67, 0.96, and 1.61 W/(m·K), respectively. The linear regression of measured thermal conductivity against known thermal conductivity results in a calibration correction specific to each needle probe.

Heat flow was calculated using thermal conductivity measured on sediments taken from a hole at the site where downhole temperature measurement tools were deployed (see "In Situ Temperature" section, this chapter). It was assumed that the geothermal gradient could be approximated by a linear regression of the downhole temperatures, and one-dimensional heat flow (Q) was computed using

$$Q = k\left(\frac{\Delta T}{\Delta z}\right),$$

where $\Delta T/\Delta z$ is a linear estimate of the geothermal gradient. Heat flow is reported in mW/m^2 and heat-flow units (1 HFU ≈41.8 mW/m^2).

Compressional-Wave Velocity

Compressional-wave velocity was measured using the Hamilton Frame velocimeter (HFV). The digital sonic velocimeter (DSV) either cracked or could not penetrate the sediment recovered during Leg 171B.

Velocity calculations are based upon the accurate measurement of the time for a 500-kHz acoustic signal to travel between a pair of piezoelectric transducers located at opposite sides of a split-sediment core or minicore.

Velocity measurements were made on two types of samples: split cores and minicores. Split-core velocities were measured perpendicular to the length of the core (transverse direction) and were corrected for the presence of the liner. Minicores ($^7/_8$-in outside diameter) were cut with a diamond coring tube perpendicular to the length of the core and were squared off using a diamond saw. *P*-wave velocity was measured perpendicular to the length of the core (transverse direction) and parallel to the length of the core (longitudinal direction). The sample thickness between the transducers was measured using a linear displacement transducer on the HFV. The HFV transducers were calibrated using the linear regression of traveltime vs. distance for a set of polycarbonate standards ranging in thickness from 20 to 50 cm. Seawater was added to the contact between the transducers and sample to improve acoustic coupling. Velocities are reported in units of kilometers per second.

Undrained Shear Strength

Undrained shear strength (S_u) was determined using the ODP motorized miniature vane-shear device (Boyce, 1976). The orange vane was selected for Leg 171B, and the spring was changed when necessary. Measurements were made only in fine-grained, soft sediments. The vane rotation rate was 90°/min, and the vane had a 1:1 blade ratio, with a dimension of 1.27 cm.

When analyzing vane test data, it is assumed that a cylinder of sediment is uniformly sheared about the axis of the vane in an undrained condition and that cohesion is the principal contributor to shear strength. Departures from these conditions include progressive cracking within and outside a failing specimen, uplift of a failing core cylinder, drainage of local pore pressures (i.e., the test can no longer be considered undrained), and stick-shift behavior. Occurrences of these conditions were recorded during Leg 171B analyses to aid data interpretation.

In sediments too stiff to measure with the vane-shear device, measurements were made with a pocket penetrometer. This penetrometer is a small, square-ended cylindrical probe that is pushed 6.4 mm into the split core. The resulting resistance is the unconfined compressive strength, which is $2S_u$. A scale directly reads out in units of kg/cm^2, and these values are converted to S_u and reported in units of kPa (1 kg/cm^2 = 98.07 kPa).

Drilling disturbance can limit the accuracy of these analyses, although the shipboard data provide an estimate of strength as well as additional low-frequency correlative data. Values of undrained shear strength are reported in units of kPa.

Overburden estimates were made by assuming that overcompacted sediment was previously in a state of normal compaction. Normalized shear strength (S_u), which is the ratio of shear strength to the effective overburden pressure (P_0'), can be used to assess the stress history of a sediment column. A normally consolidated sediment has an S_u/P_0' between 0.2 and 0.22 (Ladd et al., 1977). The overburden thickness (h) for an overconsolidated sediment column was estimated using the following equations:

$$h = \left[\frac{P_0'}{(\rho_b - \rho_{pw})g}\right] - z_{Su} \quad \text{and}$$

$$P_0' = \frac{S_u}{S_n},$$

where ρ_b is an estimate of the average bulk density of the sediment above depth z including the overburden, ρ_{pw} is the average density of pore water in the same depth interval, g is the acceleration of gravity, z_{Su} is the present depth of the normalized shear-strength maximum, S_u is the shear strength at the normalized shear-strength maximum, and S_n is the normalized shear strength typical for normally compacted sediments (0.2–0.22).

Electrical Resistivity

The Scripps Institution of Oceanography (SIO) probe, in combination with the ODP Wayne Kerr Precision Component Analyzer 6425, was used to determine resistivity during Leg 171B. The SIO probe has a linear configuration comprising two outer current electrodes and two inner potential electrodes (Wenner spread) at a spacing of 10 mm. Longitudinal and transverse resistivities were measured by inserting the probe parallel and perpendicular to the section, respectively.

The probe was inserted into the sediment until the block rested on the split-core surface. Electrical resistivity was measured by applying a 1.5-kHz, 10-mA alternating current through the two outer electrodes, which induced a potential drop that was measured across the two inner electrodes. The potential was internally converted to resistance by dividing by the instrument current, and the resistance was manually converted to resistivity by multiplying by the instrument cell constant. The cell constant is defined as the ratio of the cross sectional area to the length between the two inner electrodes, and it was determined for the SIO probe by measuring the resistance of seawater at controlled temperatures.

IN SITU TEMPERATURE MEASUREMENTS

Downhole temperature measurements were taken during Leg 171B to determine the variation of heat flow along the depth transect drilled across the Blake Nose. In situ temperature measurements were made using the Adara temperature tool as part of regular APC coring operations. These data were combined with measurements of thermal conductivity obtained from whole-core samples (see "Physical Properties" section, this chapter) to calculate heat-flow values.

Adara Temperature Measurements

The Adara tool was used to obtain in situ sediment temperature measurements during APC coring operations. The components of the

Adara tool are contained in an annulus in the coring shoe of the APC string and include a platinum temperature sensor and a data logger. The platinum resistance temperature device (RTD) is calibrated over a range of –20° to 100°C, with a resolution of 0.01°C. In operation, the coring shoe is attached to a core barrel and lowered down the pipe by wireline. The tool is typically held for 5–10 min at the mudline to equilibrate with bottom-water temperatures and is then lowered to the end of the drill string. Standard APC coring techniques are used, with the core barrel fired through the drill bit using hydraulic pressure. The Adara tool is left in the sediment for 10–15 min to obtain a temperature record. This provides a sufficiently long transient record for reliable extrapolation of the steady-state temperature. The nominal accuracy of the temperature measurement is ~0.1°C.

DOWNHOLE LOGGING

Downhole logs are used directly to determine the physical, chemical, and structural properties of formations penetrated by drilling and to complement discrete core measurements. Where core recovery is incomplete, logging data may serve as a proxy for physical properties and sedimentologic data. These data complement the discrete measurements obtained from cores and offer advantages over core-based analyses in that they are collected rapidly and represent continuous, in situ measurements of the formation.

Because the continuous nature of logs allows them to be treated as a time series, it is possible to define the periods of the cyclicity information they contain and to examine the impact of paleoclimatic change on the sedimentologic record.

Well Logging Operations

Standard well logging operations are as follows. After coring was completed, the holes were flushed of sediment fill by circulating heavy, viscous drilling fluid (sepiolite mud with seawater) through the drill pipe into the hole. The BHA was pulled up to about 60 to 100 mbsf and then run down to the bottom of the hole and finally back up to near the seafloor to condition the borehole for logging. Tool strings comprising one or more combinations of sensors were then lowered downhole by a seven-conductor wireline cable. Data from the tools were recorded in real time by the Schlumberger MAXIS 500 well site surface instrumentation. After logging, the data were transferred to a Sun workstation and Macintosh computers for preliminary shipboard correction, correlation, and interpretation. Wireline logging data are typically recorded at 15-cm depth increments. The specific depths of investigation into the formation and the vertical borehole resolution are sensor dependent (Table 12).

Logging Tool Strings

Individual logging tools were combined in three tool strings during Leg 171B: (1) porosity-density-resistivity string (triple-combo), comprising the phasor dual induction–spherically focused resistivity tool (DITE-SFL), hostile litho-density tool (HLDT), and the accelerator porosity sonde (APS); (2) Formation MicroScanner–sonic digital tool (FMS-SDT) combination; and (3) geological high-sensitivity magnetic tool (GHMT), comprising the nuclear magnetic resonance sonde (NMRS) and susceptibility magnetic sonde (SUMS). The natural gamma-ray spectrometry tool (NGT) was placed at the top of all three tool strings to provide a common basis for log correlation and depth adjustment. The LDEO temperature tool (TLT) was attached to the base of all tool strings, except the FMS and GHMT, to obtain borehole temperatures. Schematic diagrams of these standard tool strings are illustrated in Figure 8.

A brief description of the logging tools employed during Leg 171B follows. The detailed principles of operation of the various logging sensors and their geologic applications can be found in Serra (1984), Timur and Toksöz (1985), Ellis (1987), Schlumberger (1989), and Rider (1996).

Logging Tools

Natural Gamma-Ray Spectrometry Tool

The NGT measures the natural radioactivity of the formation using a sodium-iodine (NaI) scintillation crystal detector mounted inside the tool, which is held against the borehole wall by a bow spring during logging. This tool measures the number of gamma rays and the energy level of each and allows determination of the concentration of radioactive potassium (K), thorium (Th), and uranium (U) in the formation (Lock and Hoyer, 1971). Gamma rays are emitted by radioactive isotopes of ^{40}K and the ^{238}U and ^{232}Th decay series that are present in the formation. Measurements are analyzed by dividing the incident gamma-ray signature into five discrete energy windows, which correspond to the main spectral peaks for each element. The NGT also provides a measure of the total gamma-ray signature (SGR = K + U + Th) and a uranium-free measurement (CGR = K + Th). A full display of the data with SGR, CGR, Th (in ppm), U (in ppm), and K (in wet wt%) is usually provided separately. Values are recorded every 0.15 m and have a vertical resolution on the order of 0.46 m.

Because radioactive elements usually are most abundant in clay minerals, the gamma-ray curve typically is used to estimate the clay or shale content. There are rock matrices, however, for which the radioactivity ranges from moderate to extremely high values because of the presence of volcanic ash, potassic feldspar, or other radioactive minerals (Keys, 1979; Sanyal et al., 1980). U/Th ratios from NGT data are used also as an estimate of the amount of organic carbon (usually associated with high U counts) within formations and to distinguish changes in the oxidation state of diagenetic minerals (Doveton, 1994).

Accelerator Porosity Sonde

The APS consists of a neutron generator and five neutron detectors—four epithermal, one thermal—at different spacings from the source. The APS uses a miniature accelerator (minitron) that produces fast neutrons (14.4 MeV) by accelerating deuterium ions onto a tritium target. This eliminates the need for a radioactive source, as used in the compensated neutron tool (CNT). By pulsing the ion source, a pulsed source of neutrons can be produced. Neutrons travel through the surrounding borehole and formation and interact primarily with hydrogen nuclei present in the common formation fluids, water (H_2O), and oil (CH_2). Because the neutrons and hydrogen atoms have about the same mass, successive collisions reduce the energy of the neutrons to the energy level of the formation. The APS neutron de-

Table 12. Vertical resolution and depths of investigation of the logging tools employed during Leg 171B.

Tool	Vertical resolution (cm)	Investigation depth (cm)
Phasor dual induction-spherically focused resistivity tool (DITE-SFL):		
IDPH deep resistivity	200	150
IMPH medium resistivity	150	76
SFL shallow focused	59	38
Natural spectral gamma-ray tool (NGT)	46	Variable
Accelerator porosity sonde (APS)	20	15
High-temperature lithodensity tool (HLDT)	38	Variable (15-60)
Geological high-sensitivity magnetic tool (GHMT)	5	
Formation MicroScanner (FMS)	0.5	Variable (5-25)

Note: The vertical resolution, or aperture, is the minimum depth interval for which a representative log measurement can be obtained.

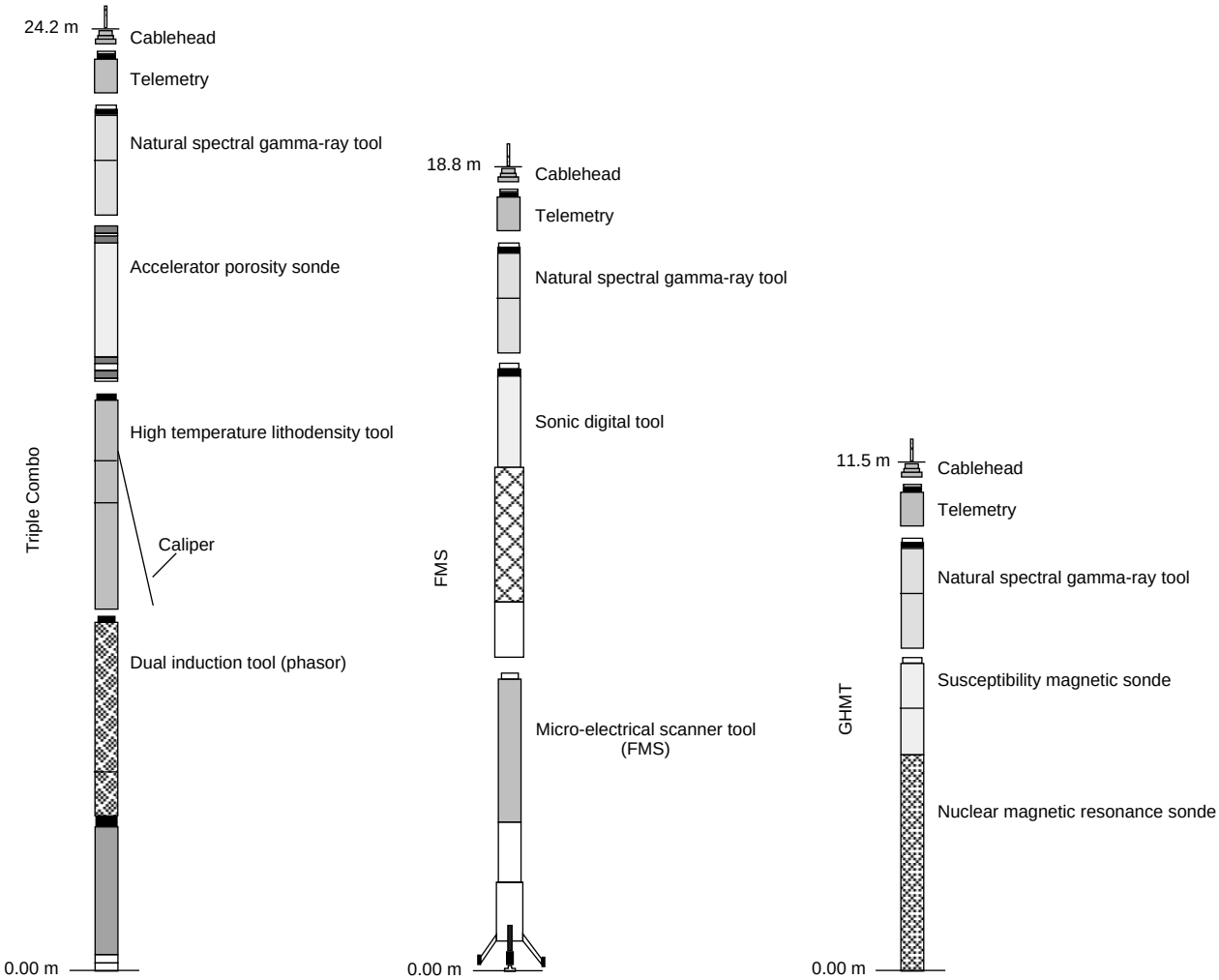

Figure 8. Schematic diagram of the logging tool strings used during Leg 171B. Tool strings are not to scale.

tector system can measure both neutron count rates and neutron arrival time. This information is used to derive an epithermal (0.1–100 eV) neutron porosity measurement of the formation, independent of thermal neutron absorbers, and a thermal (<0.025 eV) neutron measurement of the formation capture cross section (sigma).

The accuracy of neutron porosity may be adversely affected by variations in hole size that result in an increased H flux from seawater drilling fluids. The tool is held against the side of the borehole by a bow spring to reduce the effects of variations in hole diameter. The tool provides a vertical resolution of ~8 in and a shallow depth of investigation of about 6 in.

Hostile Litho-Density Tool

The HLDT uses a ^{137}Cs radioactive source and two detectors mounted on a shielded sidewall skid that is pressed against the formation by a hydraulically activated arm. The medium-energy gamma rays emitted by the source at an energy of 662 keV lose energy by interaction with the electrons in the formation, causing Compton scattering (Dewan, 1983) until they are absorbed through the photoelectric effect (PEF). The number of gamma rays reaching the two vertically spaced detectors yields an energy spectrum for each detector that is directly related to the number of electrons in the formation, which, in turn, is related to bulk density.

Photoelectric absorption occurs when the gamma rays reach a low energy (<150 keV) after being continually scattered by the electrons in the formation. The PEF depends on the atomic number of the elements in the formation; thus, the magnitude of this measurement is nearly independent of porosity. The PEF values, when used in combination with the NGT curves, can provide an indication of the different types of clay minerals in the formation. A caliper measurement is made of the borehole diameter to correct the measurements for poor contact of the detector pads with the borehole wall. The depth of resolution of the HLDT is in the range of tens of centimeters, depending on the density of the rock, and provides a vertical resolution of about 38 cm (Table 12; Fig. 8).

Phasor Dual Induction–Spherically Focused Resistivity Tool

The DITE-SFL provides values of spontaneous potential (SP) and three different measurements of electrical resistivity, each one with a different depth of investigation into the formation. Two induction devices, deep (IDPH) and medium (IMPH) resistivities, transmit high-frequency alternating currents through transmitter coils, creating magnetic fields that induce secondary (Foucault) currents in the formation. These ground-loop currents produce new inductive signals that are proportional to the conductivity of the formation, which are recorded by the receiving coils. The measured conductivities are then

converted to resistivity (in Ωm). The shallow SFL measures the current necessary to maintain a constant voltage decrease across a fixed interval in the near-borehole region. The vertical resolution is about 2 m for the medium- and deep-resistivity devices and about 1 m for the shallow-focused device. Values are recorded every 15.24 cm.

Water content and salinity are the most significant factors controlling the electrical resistivity of a formation. Resistivity is related primarily to the inverse square root of porosity (Archie, 1942). The other main factors influencing the resistivity of a formation include the concentration of hydrous and metallic minerals, hydrocarbons, and gas hydrates and the abundance, distribution, and geometry (tortuosity) of interconnected pore space.

Sonic Digital Tool

The sonic digital tool measures the time required for sound waves to travel along the borehole wall from one of two acoustic transmitters to two receivers over source-receiver distances of 2.4, 3.0, and 3.6 m. First arrivals for the individual source-receiver paths are used to calculate sonic velocities; four velocity values are measured at each depth, along four possible paths. Only compressional-wave velocities are determined on board ship, but the full sonic waveforms are recorded for post-cruise processing to determine shear-wave and Stonely-wave velocities. The standard vertical resolution is ~60 cm, although special array processing can produce a resolution of 15 cm. Logs can be corrected for cycle skipping (where the receiver misses the first arrival and responds to that of the second signal), using the fourfold measurement redundancy. Compressional-wave velocity is controlled primarily by porosity and lithification; the decrease in porosity and increase in lithification with depth typically result in a velocity increase with depth in a sedimentary deposit.

Formation MicroScanner Tool

The FMS tool is a microelectrical scanner tool that provides high-resolution images of the electrical conductivity variations along the borehole wall that can be used to reconstruct the depth position and orientation of the cores recovered. The FMS tool comprises four orthogonal imaging pads, with 16 button electrodes (6.7 mm in diameter) on each pad, that are pressed against the borehole wall (Serra, 1989). Pad electrodes are spaced about 2.5 mm apart and are arranged in two diagonally offset rows of eight electrodes each. Each pad measures about 8 cm^2, and one pass of the four-pad tool covers ~30% of the borehole wall in a 25.72-cm-diameter borehole. The tool works by emitting a focused electrical current from the four pads into the formation. The button electrode current intensity is sampled every 2.5 mm, providing a vertical resolution of ~0.5 cm (Serra, 1989). Processing transforms the current intensity measurements, which reflect the micoresistivity variations of the formation, into high-resolution images of varying color and intensity. The FMS tool string includes a general purpose inclinometry tool (GPIT) that orients the resistivity measurements through the use of an accelerometer and magnetometer that respond to the declination and inclination of the Earth's magnetic field.

FMS images can be used for the detailed correlation of coring and logging depths; core orientation; mapping of fractures, faults, foliations, and other formation structures; as well as determination of strikes and dips of bedding planes (Ekstrom et al., 1987). Sedimentary structures, such as slumps, laminations, and bedding, can also be imaged.

Geological High-Sensitivity Magnetometer Tool

The GHMT string comprises the NMRS high-sensitivity total magnetic field sensor coupled with the SUMS, which are used to detect borehole magnetic polarity transitions and susceptibility variations, respectively. The NMRS measures the frequency of proton precession between a calibrated applied polarizing field and the Earth's magnetic field that is proportional to the total field intensity of the Earth. The average precision of 0.5 nT is based on duplicate runs, and the sensitivity is about 10^{-2} nT. The SUMS detects the mutual induction signal between two coils (0.8 m apart) caused by the surrounding borehole lithology. The excitation frequency is about 200 Hz. The precision between duplicate runs is generally better than 3×10^{-6} SI, and the sensitivity of the sonde is almost 10^{-6} units. Logging data are recorded every 5 cm, with a vertical resolution of ~5 cm.

Specifications of the probes, such as impulse response, calibration ratio, and geomagnetic location of the hole, are used to calculate the susceptibility effect on the scalar total-field magnetometer. From these data, the scalar remanent magnetization can be calculated. Results from borehole measurement of the magnetic reversal sequence (MRS) can be correlated with the geomagnetic polarity time scale (GPTS) for absolute formation dating, giving a formation depth-to-age conversion.

Lamont-Doherty Temperature Tool

The LDEO TLT is a high-precision, low-temperature, self-contained logging tool that can be attached to the bottom of any Schlumberger tool string to record borehole temperatures. Data from two types of thermistors (fast and slow response times) and a pressure transducer are collected at a predetermined rate of one sample every 0.5–5.0 s and are stored internally. The fast-response, lower accuracy thermistor (time constant ~0.4 s, precision 0.005°C) has the capacity to detect small, abrupt temperature excursions in the borehole fluids that may be caused by fluid flow from the formation. The slow-response, higher accuracy thermistor also has a precision of 0.005°C and can be used to estimate borehole fluid temperature. Data are recorded as a function of time, with conversion to depth based on pressure recordings from the pressure transducer and on the synchronized time-depth record of the wireline cable. The data recorded by the TLT are unlikely to match equilibrated formation temperatures because drilling and circulation operations disturb the temperature conditions in the borehole. However, with the spatial temperature gradient, it is possible to identify abrupt gradient changes that may indicate localized fluid flow between the borehole and the formation.

Log Data Quality

Log data quality may be seriously degraded by abrupt changes in the hole diameter and in sections where the borehole diameter is greatly increased or washed out. Deep investigation devices, such as the resistivity and velocity tools, are the least sensitive to borehole effect, whereas nuclear measurements (density, neutron porosity, and both natural and induced spectral gamma ray) are more sensitive because of their shallower depth of investigation and of the effect of the increased fluid volume on neutron and gamma-ray attenuation. Although corrections can be made to the original data to reduce these effects, they cannot account for very large washouts.

Small depth mismatches between logging runs in a single hole can impair the logging results in zones of abruptly changing lithology. During Leg 171B, the hydraulic wireline heave compensator (WHC), which adjusts for rig motion during logging operations, was not in service; consequently, logs taken during periods of significant ship heave may be degraded and may have required additional processing and correction (see individual site chapters).

Log Processing and Analysis

After logging, data are processed and reformatted on board ship to display the preliminary downhole measurements. Shore-based processing of data from each logging hole, using Schlumberger

Logos software and additional programs developed by LDEO-BRG, includes (1) depth adjustments of all logs to a common mbsf measurement, (2) corrections specific to certain tools, and (3) quality control and the rejection of unrealistic or spurious values. Files of all processed logs (including FMS, dipmeter, high-resolution density, and neutron data), sonic waveforms, and explanatory text are included on CD-ROM (back pocket, this volume). All data can be obtained from LDEO-BRG.

REFERENCES

Archie, G.E., 1942. The electrical resistivity log as an aid in determining some reservoir characteristics. *J. Pet. Technol.*, 5:1–8.

Aubry, M.-P., Berggren, W.A., Kent, D.V., Flynn, J.J., Klitgord, K.D., Obradovich, J.D., and Prothero, D.R., 1988. Paleogene geochronology: an integrated approach. *Paleoceanography*, 3:707–742.

Backman, J., 1986. Late Paleocene to middle Eocene calcareous nannofossil biochronology from the Shatsky Rise, Walvis Ridge and Italy. *Palaeogeogr., Palaeoclimatol., Palaeoecol.*, 57:43–59.

————, 1987. Quantitative calcareous nannofossil biochronology of middle Eocene through early Oligocene sediment from DSDP Sites 522 and 523. *Abh. Geol. Bundesanst. (Austria)*, 39:21–31.

Barker, C.E., and Pawlewicz, M.J., 1993. Calculation of vitrinite reflectance from thermal histories and peak temperature: a comparison of methods. *In* Mukhopadhyay, P.K., and Dow, W.G. (Eds.), *Vitrinite Reflectance as a Maturity Parameter.* Am. Chem. Soc. Symp. Ser., 570:216–229.

Barron, J.A., 1989. The late Cenozoic stratigraphic record and hiatuses of the northeast Pacific: results from the Deep Sea Drilling Project. *In* Winterer, E.L., Hussong, D.M., and Decker, R.W. (Eds.), *The Geology of North America* (Vol. N): *The Eastern Pacific Ocean and Hawaii.* Geol. Soc. Am., Geol. of North America Ser., 311–322.

Basov, I.A., and Krasheninnikov, V.A., 1983. Benthic foraminifers in Mesozoic and Cenozoic sediments of the southwestern Atlantic as an indicator of paleoenvironment, Deep Sea Drilling Project Leg 71. *In* Ludwig, W.J., Krasheninnikov, V.A., et al., *Init. Repts. DSDP,* 71: Washington (U.S. Govt. Printing Office), 739–788.

Bellier, J.-P., 1983. Foraminiferes Planctoniques du Cretace de Tunisie septentrionale: utilisation stratigraphique des formes trochospiralees de l'Albien au Maastrichtien. *Mem. Soc. Geol. Fr.*, 146:70.

Benson, W.E., Sheridan, R.E., et al., 1978. *Init. Repts. DSDP,* 44: Washington (U.S. Govt. Printing Office).

Berggren, W.A., Kent, D.V., and Flynn, J.J., 1985a. Jurassic to Paleogene, Part 2. Paleogene geochronology and chronostratigraphy. *In* Snelling, N.J. (Ed.), *The Chronology of the Geological Record.* Geol. Soc. London Mem., 10:141–195.

Berggren, W.A., Kent, D.V., Swisher, C.C., III, and Aubry, M.-P., 1995. A revised Cenozoic geochronology and chronostratigraphy. *In* Berggren, W.A., Kent, D.V., Aubry, M.-P., and Hardenbol, J. (Eds.), *Geochronology, Time Scales and Global Stratigraphic Correlation.* Spec. Publ.—Soc. Econ. Paleontol. Mineral., 54:129–212.

Berggren, W.A., Kent, D.V., and Van Couvering, J.A., 1985b. The Neogene, Part 2. Neogene geochronology and chronostratigraphy. *In* Snelling, N.J. (Ed.), *The Chronology of the Geological Record.* Geol. Soc. London Mem., 10:211–260.

Berggren, W.A., and Miller, K.G., 1988. Paleogene tropical planktonic foraminiferal biostratigraphy and magnetobiochronology. *Micropaleontology,* 34:362–380.

Bolli, H.M., Saunders, J.B., and Perch-Nielsen, K. (Eds.), 1985. *Plankton Stratigraphy:* Cambridge (Cambridge Univ. Press).

Bordenave, M.L., Espitalie, J., Leplat, P., Oudin, J.L., and Vandenbroucke, M., 1993. Screening techniques for source rock evaluation. *In* Bordenave, M.L. (Ed.), *Applied Petroleum Geochemistry:* Paris (Editions Technip), 217–279.

Boyce, R.E., 1976. Definitions and laboratory techniques of compressional sound velocity parameters and wet-water content, wet-bulk density, and porosity parameters by gravimetric and gamma-ray attenuation techniques. *In* Schlanger, S.O., Jackson, E.D., et al., *Init. Repts. DSDP,* 33: Washington (U.S. Govt. Printing Office), 931–958.

Bukry, D., 1973. Low-latitude coccolith biostratigraphic zonation. *In* Edgar, N.T., Saunders, J.B., et al., *Init. Repts. DSDP,* 15: Washington (U.S. Govt. Printing Office), 685–703.

————, 1975. Coccolith and silicoflagellate stratigraphy, northwestern Pacific Ocean, Deep Sea Drilling Project Leg 32. *In* Larson, R.L., Moberly, R., et al., *Init. Repts. DSDP,* 32: Washington (U.S. Govt. Printing Office), 677–701.

Bustin, R.M., Cameron, A.R., Grieve, D.A., and Kalkreuth, W.D., 1983. Coal petrology: its principles, methods and applications. *Geol. Soc. Can., Short Course Notes,* 3.

Bybell, L.M., and Self-Trail, J.M., 1995. Evolutionary, biostratigraphic, and taxonomic study of calcareous nannofossils from a continuous Paleocene/Eocene boundary section in New Jersey. *Geol. Surv. Prof. Pap. U.S.*, 1554.

Cande, S.C., and Kent, D.V., 1995. Revised calibration of the geomagnetic polarity timescale for the Late Cretaceous and Cenozoic. *J. Geophys. Res.*, 100:6093–6095.

Cardoso, J.N., Wardroper, A.M.K., Watts, C.D., Barnes, J.R., Maxwell, J.R., Eglinton, G., Mound, D.G., and Speers, G.C., 1978. Preliminary organic geochemical analyses, Site 391, Leg 44 of the Deep Sea Drilling Project. *In* Benson, W.E., and Sheridan, R.E, et al., *Init. Repts. DSDP,* 44: Washington (U.S. Govt. Printing Office), 617–624.

Caron, M., 1985. Cretaceous planktic foraminifera. *In* Bolli, H.M., Saunders, J.B., and Perch-Nielsen, K. (Eds), *Plankton Stratigraphy:* Cambridge (Cambridge Univ. Press), 17–86.

Chaisson, W.P., and Leckie, R.M., 1993. High-resolution Neogene planktonic foraminifer biostratigraphy of Site 806, Ontong Java Plateau (western equatorial Pacific). *In* Berger, W.H., Kroenke, L.W., Mayer, L.A., et al., *Proc. ODP, Sci. Results,* 130: College Station, TX (Ocean Drilling Program), 137–178.

Curry, W.B., Shackleton, N.J., Richter, C., et al., 1995. *Proc. ODP, Init. Repts.*, 154: College Station, TX (Ocean Drilling Program).

Dewan, J.T., 1983. *Essentials of Modern Open-Hole Log Interpretation:* Tulsa (PennWell).

Doeglas, D.J., 1968. Grain-size indices, classification and environment. *Sedimentology,*10:83–100.

Doveton, J.H., 1994. Geologic log interpretation. *SEPM Short Course,* 29:33–36.

Dow, W.G., 1978. Geochemical analysis of samples from holes 391A and 391C, Leg 44, Blake-Bahama Basin. *In* Benson, W.E., and Sheridan, R.E, et al., *Init. Repts. DSDP,* 44: Washington (U.S. Govt. Printing Office), 625–634.

Dunham, R.J., 1962. Classification of carbonate rocks according to depositional texture. *In* Ham, W.E. (Ed.), *Classification of Carbonate Rocks.* AAPG Mem., 108–121.

Ekstrom, M.P., Dahan, C., Chen, M.-Y., Lloyd, P., and Rossi, D.J., 1987. Formation imaging with microelectrical scanning arrays. *Log Analyst,* 28:294–306.

Ellis, D.V., 1987. *Well Logging for Earth Scientists:* New York (Elsevier).

Emeis, K.-C., and Kvenvolden, K.A., 1986. Shipboard organic geochemistry on *JOIDES Resolution. ODP Tech. Note,* 7.

Erba, E., Premoli Silva, I., and Watkins, D.K., 1995. Cretaceous calcareous plankton biostratigraphy of Sites 872 through 879. *In* Haggerty, J.A., Premoli Silva, I., Rack, F., and McNutt, M.K. (Eds.), *Proc. ODP, Sci. Results,* 144: College Station, TX (Ocean Drilling Program), 157–169.

Espitalié, J., Deroo, G., and Marquis, F., 1986. La pyrolyse Rock-Eval et ses applications, Partie III. *Rev. Inst. Fr. Pet.*, 41:73–89.

Foreman, H.P., 1968. Upper Maestrichtian Radiolaria of California. *Palaeontol. Assoc. London, Spec. Pap. Palaeontol.*, 3:1–82.

Gartner, S., 1992. Miocene nannofossil chronology in the North Atlantic, DSDP Site 608. *Mar. Micropaleontol.*, 18:307–331.

Gieskes, J.M., Gamo, T., and Brumsack, H., 1991. Chemical methods for interstitial water analysis aboard *JOIDES Resolution. ODP Tech. Note,* 15.

Gradstein, F.M., 1978. Biostratigraphy of Lower Cretaceous Blake Nose and Blake Bahama Basin foraminifera, DSDP Leg 44, western North Atlantic Ocean. *In* Benson, W.E., Sheridan, R.E., et al., *Init. Repts. DSDP,* 44: Washington (U.S. Govt. Printing Office), 663–702.

Gradstein, F.M., Agterberg, F.P., Ogg, J.G., Hardenbol, J., van Veen, P., Thierry, J., and Huang, Z., 1995. A Triassic, Jurassic and Cretaceous time scale. *In* Berggren, W.A., Kent, D.V., and Aubry, M.P. (Eds.), *Geochronology, Time Scales and Global Stratigraphic Correlation.* Spec. Publ.—Soc. Econ. Paleontol. Mineral., 54:95–128.

Gutjahr, C.C.M., 1983. Introduction to incident-light microscopy of oil and gas source rocks. *Geol. Mijnbouw,* 62:417–425.

Hagelberg, T., Shackleton, N., Pisias, N., and Shipboard Scientific Party, 1992. Development of composite depth sections for Sites 844 through 854. *In* Mayer, L., Pisias, N., Janecek, T., et al., *Proc. ODP, Init. Repts.*, 138 (Pt. 1): College Station, TX (Ocean Drilling Program), 79–85.

Hagelberg, T.K., Pisias, N.G., Shackleton, N.J., Mix, A.C., and Harris, S., 1995. Refinement of a high-resolution, continuous sedimentary section for studying equatorial Pacific Ocean paleoceanography, Leg 138. *In* Pisias, N.G., Mayer, L.A., Janecek, T.R., Palmer-Julson, A., and van Andel, T.H. (Eds.), *Proc. ODP, Sci Results*, 138: College Station, TX (Ocean Drilling Program), 31–46.

Harris, S., Hagelberg, T., Mix, A., Pisias, N., and Shackleton, N.J., 1995. Sediment depths determined by comparisons of GRAPE and logging density data during Leg 138. *In* Pisias, N.G., Mayer, L.A., Janecek, T.R., Palmer-Julson, A., and van Andel, T.H. (Eds.), *Proc. ODP, Sci. Results*, 138: College Station, TX (Ocean Drilling Program), 47–57.

Holbrook, W.S., Hoskins, H., Wood, W.T., Stephen, R.A., Lizzarralde, D., and the Leg 164 Science Party, 1996. Methane gas-hydrate and free gas on the Blake Ridge from vertical seismic profiling. *Science*, 273:1840–1843.

Hollis, C.J., 1993. Latest Cretaceous to Late Paleocene radiolarian biostratigraphy: a new zonation from the New Zealand region. *Mar. Micropaleontol.*, 21:295–327.

Jud, R., 1994. Biochronology and systematics of Early Cretaceous radiolaria of the Western Tethys. *Mem. Geol. (Lausanne)*, 19:1–147.

Katz, B.J., 1983a. Limitations of "Rock-Eval" pyrolysis for typing organic matter. *Org. Geochem.*, 4:195–199.

————, 1983b. Organic geochemical character of some Deep Sea Drilling Project cores from Legs 76 and 44. *In* Sheridan, R.E., Gradstein, F.M., et al., *Init. Repts. DSDP*, 76: Washington (U.S. Govt. Printing Office), 463–468.

Kennett, J.P., and Srinivasan, M.S., 1983. *Neogene Planktonic Foraminifera: A Phylogenetic Atlas:* Stroudsburg, PA (Hutchinson Ross).

Keys, W.S., 1979. Borehole geophysics in igneous and metamorphic rocks. *Trans. SPWLA 20th Annu. Logging Symp.*, Pap. OO, 1–26.

Kvenvolden, K.A., and McDonald, T.J., 1986. Organic geochemistry on the *JOIDES Resolution*—an assay. *ODP Tech. Note*, 6.

Kvenvolden, K.A., and McMenamin, M.A., 1980. Hydrates of natural gas: a review of their geologic occurrence. *Geol. Surv. Circ. (U.S.)*, 825.

Ladd, D.D., Foott, R., Ishihara, K., Schlosser, F., and Poulos, H.G., 1977. Stress-deformation and strength characteristics: state-of-the-art report. *Proc. 9th Int. Conf. Soil Mechanics Foundation Engineering*, Tokyo, 2:421–482.

Langford, F.F., and Blanc-Valleron, M.M., 1990. Interpreting Rock-Eval pyrolysis data using graphs of pyrolizable hydrocarbons vs. total organic carbon. *AAPG Bull.*, 74:799–804.

Lock, G.A., and Hoyer, W.A., 1971. Natural gamma-ray spectral logging. *Log Analyst*, 12:3–9.

Mayer, L., Pisias, N., Janecek, T., et al., 1992. *Proc. ODP, Init. Repts.*, 138 (Pts. 1 and 2): College Station, TX (Ocean Drilling Program).

Mazzullo, J.M., Meyer, A., and Kidd, R.B., 1988. New sediment classification scheme for the Ocean Drilling Program. *In* Mazzullo, J., and Graham, A.G. (Eds.), *Handbook for Shipboard Sedimentologists.* ODP Tech. Note, 8:45–67.

Moore, D.M., and Reynolds, R.C., Jr., 1989. *X-ray Diffraction and the Identification and Analysis of Clay Minerals:* Oxford (Oxford Univ. Press).

Moran, K., 1997. Elastic property corrections applied to Leg 154 sediment, Ceara Rise. *In* Shackleton, N.J., Curry, W.B., Richter, C., and Bralower, T.J. (Eds.), *Proc. ODP, Sci. Results*, 154: College Station, TX (Ocean Drilling Program), 151–155.

Munsell Color Company, Inc., 1975. *Munsell Soil Color Charts:* Baltimore, MD (Munsell).

Nederbragt, A.J., 1991. Late Cretaceous biostratigraphy and development of Heterohelicidae planktic foraminifera. *Micropaleontology*, 37:329–372.

Norrish, K., and Hutton, J.T., 1969. An accurate X-ray spectrographic method for the analysis of a wide range of geological samples. *Geochim. Cosmochim. Acta*, 33:431–453.

O'Dougherty, L., 1994. Biochronology and paleontology of middle Cretaceous radiolarians from Umbria-Marche Appennines (Italy) and Betic Cordillera (Spain). *Mem. Geol. Lausanne*, 21:1–351.

Okada, H., and Bukry, D., 1980. Supplementary modification and introduction of code numbers to the low-latitude coccolith biostratigraphic zonation (Bukry, 1973; 1975). *Mar. Micropaleontol.*, 5:321–325.

Olsson, R.K., Berggren, W.A., Hemleben, C., Huber, B.T., and the Paleogene Planktonic foraminiferal working group, in press. Atlas of Paleocene planktonic foraminifera. *Smithsonian Contrib. Paleobiol.*

Paull, C.K., Matsumoto, R., Wallace, P.J., et al., 1996. *Proc. ODP, Init. Repts.*, 164: College Station, TX (Ocean Drilling Program).

Pawlewicz, M.J., 1986. Polishing method for dispersed vitrinite and coal slides. *Soc. Org. Petrol. Newsl.*, 5:3.

Perch-Nielsen, K., 1985. Mesozoic calcareous nannofossils. *In* Bolli, H.M., Saunders, J.B., and Perch-Nielsen, K. (Eds.), *Plankton Stratigraphy:* Cambridge (Cambridge Univ. Press), 329–426.

Pessagno, E.A., 1976. Radiolarian zonation and stratigraphy of the Late Cretaceous portion of the Great Valley Sequence, California Coast Range. *Micropaleontology, Spec. Publ.*, 2:1–95.

————, 1977. Lower Cretaceous Radiolarian biostratigraphy of the Great Valley sequence and Franciscan Complex, California Coast Ranges. *Spec. Publ. Cushman Found. Foraminiferal Res.*, 15:5–87.

Peters, K.E., 1986. Guidelines for evaluating petroleum source rock using programmed pyrolysis. *AAPG Bull.*, 70:318–329.

Raffi, I., and Flores, J.-A., 1995. Pleistocene through Miocene calcareous nannofossils from eastern equatorial Pacific Ocean (Leg 138). *In* Pisias, N.G., Mayer, L.A., Janecek, T.R., Palmer-Julson, A., and van Andel, T.H. (Eds.), *Proc. ODP, Sci. Results*, 138: College Station, TX (Ocean Drilling Program), 233–286.

Rider, M., 1996. *The Geological Interpretation of Well Logs:* Caithness (Whittles Publishing).

Riedel, W.R., and Sanfilippo, A., 1978. Stratigraphy and evolution of tropical Cenozoic radiolarians. *Micropaleontology*, 24:61–96.

Robaszynski, F., and Caron, M., 1979. Atlas de foraminiferes planctoniques du Cretace moyen (Mer Boreale et Tethys) (Vols. 1 and 2). *Cah. Micropaleontol.*

Robaszynski, F., Caron, M., Gonzales-Donoso, J.-M., Wonders, A.A.H., and the European Working Group on Planktonic Foraminifera, 1984. Atlas of Late Cretaceous globotruncanids. *Rev. Micropaleontol.*, 26:145–305.

Robert, P., 1988. *Organic Metamorphism and Geothermal History:* Dordrecht (D. Reidel).

Rock-Color Chart Committee, 1991. *Rock Color Charts.* Geol. Soc. Am.

Rothwell, R.G., 1989. *Minerals and Mineraloids in Marine Sediments: An Optical Identification Guide:* Basking, UK (Elsevier Appl. Sci. Publ.).

Sanfilippo, A., and Riedel, W.R., 1985. Cretaceous radiolaria. *In* Bolli, H.M., Saunders, J.B., and Perch-Nielsen, K. (Eds.), *Plankton Stratigraphy:* Cambridge (Cambridge Univ. Press), 573–630.

Sanfilippo, A., Westberg-Smith, M.J., and Riedel, W.R., 1985. Cenozoic radiolaria. *In* Bolli, H.M., Saunders, J.B., and Perch-Nielsen, K. (Eds.), *Plankton Stratigraphy:* Cambridge (Cambridge Univ. Press), 631–712.

Sanyal, S.K., Jupraset, S., and Jusbasche, M., 1980. An evaluation of a rhyolite basaltic volcanic ash sequence from well logs. *Log Analyst*, 21:10–23.

Schaaf, A., 1981. Late Early Cretaceous radiolarians from Deep Sea Drilling Project Leg 62. *In* Thiede, J., Vallier, T.L., et al., *Init. Repts. DSDP*, 62: Washington (U.S. Govt. Printing Office), 419–470.

————, 1984. Les radiolaires du Cretace Inferiuer et Moyen: biologie et systematiques. *Sci. Geol. Mem.*, 75:1–189.

Schlumberger, 1989. *Log Interpretation Principles/Applications:* Houston, TX (Schlumberger Educ. Services).

Serra, O., 1984. *Fundamentals of Well-Log Interpretation* (Vol. 1): *The Acquisition of Logging Data:* Dev. Pet. Sci., 15A: Amsterdam (Elsevier).

————, 1989. *Formation MicroScanner Image Interpretation:* Houston (Schlumberger Educ. Services), SMP-7028.

Shipboard Scientific Party, 1992. Explanatory notes. *In* Davis, E.E., Mottl, M.J., Fisher, A.T., et al., *Proc. ODP, Init. Repts.*, 139: College Station, TX (Ocean Drilling Program), 55–97.

————, 1996. Explanatory notes. *In* Jansen, E., Raymo, M.E., Blum, P., et al., *Proc. ODP, Init. Repts.*, 162: College Station, TX (Ocean Drilling Program), 21–45.

————, 1997. Explanatory notes. *In* Kimura, G., Silver, E., Blum, P., et al., *Proc. ODP, Init. Repts.*, 170: College Station, TX (Ocean Drilling Program), 19–42.

Sigurdsson, H., Leckie, R.M., Acton, G.D., et al., 1997. *Proc. ODP, Init. Repts.*, 165: College Station, TX (Ocean Drilling Program).

Sissingh, W., 1977. Biostratigraphy of Cretaceous calcareous nannoplankton. *Geol. Mijnbouw*, 56:37–65.

Stach, E., Mackowsky, M.-T., Teichmüller, M., Taylor, G.H., Chandra, D., and Teichmüller, R., 1982. *Stach's Textbook of Coal Petrology* (3rd ed.): Berlin (Gebrüder Borntraeger).

Timur, A., and Toksöz, M.N., 1985. Downhole geophysical logging. *Annu. Rev. Earth Planet. Sci.*, 13:315–344.

Tissot, B.P., Deroo, G., and Herbin, J.P., 1979. Organic matter in Cretaceous sediments of the north Atlantic: contributions to sedimentology and paleogeography. *In* Talwani, M., Hay, W., and Ryan, W.B.F. (Eds.), *Deep Drilling Results in the Atlantic Ocean: Continental Margins and Paleoenvironment*s. Am. Geophys. Union, 362–376.

Tissot, B.P., Pelet, R., and Ungerer, P., 1987. Thermal history of sedimentary basins, maturation indices and kinetics of oil and gas generation. *AAPG Bull.*, 71:1445–1466.

Tissot, B.P., and Welte, D.H., 1984. *Petroleum Formation and Occurrence* (2nd ed.): Heidelberg (Springer-Verlag).

Tjalsma, R.C., and Lohmann, G.P., 1983. Paleocene-Eocene bathyal and abyssal benthic foraminifera from the Atlantic Ocean. *Micropaleontol. Spec. Publ.,* 4.

Toumarkine, M., and Luterbacher, H., 1985. Paleocene and Eocene planktic foraminifera. *In* Bolli, H.M., Saunders, J.B., and Perch-Nielsen, K. (Eds.), *Plankton Stratigraphy:* Cambridge (Cambridge Univ. Press), 87–154.

van Morkhoven, F.P.C.M., Berggren, W.A., and Edwards, A.S., 1986. Cenozoic cosmopolitan deep-water benthic foraminifera. *Bull. Cent. Rech. Explor.—Prod. Elf-Aquitaine,* Mem. 11.

Von Herzen, R.P., and Maxwell, A.E., 1959. The measurement of thermal conductivity of deep-sea sediments by a needle-probe method. *J. Geophys. Res.,* 64:1557–1563.

Wentworth, C.K., 1922. A scale of grade and class terms of clastic sediments. *J. Geol.,* 30:377–392.

Widmark, J.G.V., 1997. Deep-sea benthic foraminifera from Cretaceous/Tertiary boundary strata in the South Atlantic Ocean: taxonomy and paleoecology. *Fossils Strata,* 43:1–94.

Ms 171BIR-102